SPIN COATED COPPER (I) THIOCYANATE AS A HOLE TRANSPORT
LAYER FOR PEROVSKITE SOLAR CELLS

A THESIS SUBMITTED TO
THE GRADUATE SCHOOL OF NATURAL AND APPLIED SCIENCES
OF
MIDDLE EAST TECHNICAL UNIVERSITY

BY

UTKU ER

IN PARTIAL FULFILLMENT OF THE REQUIREMENTS
FOR
THE DEGREE OF MASTER OF SCIENCE
IN
METALLURGICAL AND MATERIALS ENGINEERING

MAY 2018

Approval of the thesis:

SPIN COATED COPPER (I) THIOCYANATE AS A HOLE TRANSPORT LAYER FOR PEROVSKITE SOLAR CELLS

submitted by **UTKU ER** in partial fulfillment of the requirements for the degree of **Master of Science in Metallurgical and Materials Engineering Department, Middle East Technical University** by,

Prof. Dr. Halil Kalıpçılar   _____
Dean, Graduate School of **Natural and Applied Sciences**

Prof. Dr. C. Hakan Gür   _____
Head of Department, **Metallurgical and Materials Engineering**

Prof. Dr. Ahmet Macit Özenbaş   _____
Supervisor, **Metallurgical and Materials Eng. Dept**., METU

Examining Committee Members:

Prof. Dr. Abdullah Öztürk   _____
Metallurgical and Materials Eng. Dept., METU

Prof. Dr. Ahmet Macit Özenbaş   _____
Metallurgical and Materials Eng. Dept., METU

Prof. Dr. Amdulla Mekhrabov   _____
Metallurgical and Materials Eng. Dept., METU

Asst. Prof. Dr. Bilge İmer   _____
Metallurgical and Materials Eng. Dept., METU

Asst. Prof. Dr. Kazım Tur   _____
Metallurgical and Materials Eng. Dept., Atılım University

Date: _____

I hereby declare that all information in this document has been obtained and presented in accordance with academic rules and ethical conduct. I also declare that, as required by these rules and conduct, I have fully cited and referenced all material and results that are not original to this work.

Name, Last name :   UTKU, ER

Signature :

ABSTRACT

SPIN COATED COPPER (I) THIOCYANATE AS A HOLE TRANSPORT LAYER FOR PEROVSKITE SOLAR CELLS

Utku ER

M.Sc, Department of Metallurgical and Materials Engineering

Supervisor : Prof. Dr. A. Macit ÖZENBAŞ

May 2018, 76 pages

The solar energy is one of the most studied alternatives of clean and renewable energy source worldwide, while current developments and applications are highly promising. Although current applications with Si-based solar cells show higher efficiency relative to other photovoltaic systems such as the Perovskite Solar Cells (PSCs), the necessity of the Si-based solar cells on high illumination of solar radiation and expenditure of the production of those have pulled back the interest on the PSCs. Due to their proper electical and optical properties organo-lead halide perovskites have allured much attention for solar cell applications. To date; efficiencies of perovskite solar cells (PSCs) greater than 20% have been performed only with organic hole-transporting materials. However, the organic hole-transporting materials used are normally quite expensive due to complicated synthetic procedure or high-purity requirements. In this work, we indicate the application of a cheap and efficient p-type inorganic hole-transporting material, copper thiocyanate, on mesoporous n-i-p configurated perovskite based devices. A power conversion efficiency exceeding 10% was succeeded under full sun illumination with low-temperature solution process for deposition of CuSCN and a

fast solvent removal method allowed the creation of compact, highly conformal CuSCN layers that facilitate rapid carrier extraction and collection. This work performs a well defined cell configuration with optimized layers of the cell, and give excitement for utilization of cheap and abundant material for photovoltaic applications.

Keywords : Perovskite solar cells, n-i-p mesoporous structure, copper thiocyanide thin film, hole transport material.

ÖZ

PEROVSKİT GÜNEŞ HÜCRELERİ İÇİN BOŞLUK TAŞIYICI KATMAN OLARAK SPİN KAPLAMA İLE OLUŞTURULMUŞ BAKIR TİYOSİYANAT

ER, Utku

Y.Lisans, Metalurji ve Malzeme Mühendisliği Bölümü

Tez Danışmanı : Prof. Dr. A. Macit ÖZENBAŞ

Mayıs 2018, 76 sayfa

Güneş enerjisi, üzerinde en çok çalışma yapılan temiz ve yenilenebilir enerji kaynaklarından biridir ve bu konuda yapılan güncel çalışmalar ve gelişmeler umut vaat edicidir. Si-temelli güneş hücreleri, perovskit güneş hücreleri gibi diğer fotovoltaik sistemlerle kıyaslandığında daha yüksek verime sahip olmasına rağmen, Si-temelli bu hücrelerin güneş altında yüksek aydınlatmaya ve üretim masraflarına ihtiyaç duyması, perovskit güneş hücrelerine olan ilgiyi arttırmıştır. Perovskit malzemeler, uygun optik ve elektriksel özelliklerinden dolayı güneş hücresi uygulamalarında cezbedici öneme sahiptir. Bu güne kadar, perovskit güneş hücrelerinin verimleri %20 nin üzerinde performansa sadece organik boşluk taşıyıcı malzemelerin kullanımı ile ulaşmıştır. Fakat, organik boşluk taşıyıcı malzemeler; onların karmaşık sentetik üretim metodları ve yüksek saflık gerekliliklerinden dolayı oldukça pahalıdır. Bu çalışmada; mezo gözenekli n-i-p yapıda perovskit aygıtlarda ucuz ve verimli bir p tipi inorganik boşluk taşıycı malzeme olan Bakır Tiyosiyanat'ın uygulaması gösterilmiştir. Bakır Tiyosiyanat'ın düşük sıcaklıkta çözelti prosesi ve hızlı çözücü uçurma metodu ile kaplanması sayesinde yoğun ve uygun Bakır Tiyosiyanat katmanı oluşturulması ile tam güneş aydınlatması altında güç dönüştürme veriminin %10'un üzerine çıkarılması başarılmıştır. Bu çalışmada,

hücre katmanları optimize edilerek hücre yapısı tanımlanmıştır ve fotovoltaik uygulamalarında ucuz ve bol bulunan bir malzemenin kullanımı gerçekleştirilmiştir.

Anahtar Kelimeler : Perovskit güneş hücreleri, n-i-p mezo gözenekli yapı, bakır tiyosiyanat ince film, boşluk taşıyıcı katman.

To my family...

ACKNOWLEDGMENTS

TABLE OF CONTENTS

LIST OF TABLES

LIST OF FIGURES

FIGURES

xvi

CHAPTER 1

INTRODUCTION

Reaching outstanding power converson efficiencies about 20%, perovskite solar cells have been novelty photovoltaic devices nowadays [1,2]. Cheaper raw materials and easy production procedures for fabrication are significant features of perovskite devices make attractive for photovoltaic (PV) investments and researchers and scientists all around the world. In basic structure of these devices, the architecture is determined by multilayer batch of light absorber perovskite layer that sandwiched between hole and electron transporting contact materials. Many studies like solvent engineering [3,4], additive assisted deposition [5,6] and two step deposition process [7,8] have centered on preparation of dense perovskite layers void and crack free with higher grain sizes and various preparation techniques have been improved generating grain sizes level up to millimeter. To achieve stable and highly enhanced efficiency perovskite solar devices, compostional engineering approaches [9] modifying the band positions of the perovskite layers and particular analysis of defect structure for succeeding non-defect perovskite layers with suitable additive materials [10]. Other than engineering and feverish studying of the perovskite layer, in turn energy harvesting, charge transport layers play a significant role in extracting charge carriers from perovskite absorber layer. Former studies proved that engineering of the charge extraction layers is an important parameter in order to achieve efficient charge collection and reach to the maximum photovoltage gain from the solar cell [11-13]. In perovskite solar cells, especially metal oxide semiconductors like ZnO and TiO_2 are n-type electron transport layers for n-i-p construction when counter p-type hole transport layers are especially polymeric materials such as spiro-OMeTAD, MEH-PPV, and P3HT [14]. Although high efficiency values can be provided by organic conjugacy, the dilemma is higher costs of these materials and the long term instability. p-type inorganic metal oxide layers present abundance and long term stability when collaborated in optoelectronic devices including OLEDs [15] as well as organic solar cells [16].

1

Use of inorganic hole transport materials (such as NiO, CuI, Cs_2SnI_6, and CuSCN) provide an opportunity to stable photo current efficiencies of 20% with perovskite solar cells when subjected to light soaking under realistic operational conditions [17-21]. Especially, CuSCN is an extremely cheap and abundant p-type semiconductor which exhibits good thermal stability high hole mobility, and a well-aligned work function among various inorganic HTMs [21]. CuSCN is intrinsically p-doped material, and it has high light transmission across the whole visible and near infrared spectral region, therefore it is also charming for tandem solar cell applications where the perovskite solar cell is positioned on top of a semiconductor with a lower band gap [23]. However, devices based on the standart spiro-OMETAD gives still better photocurrent efficiency values than reported with CuSCN. CuSCN layer have already reached 20% efficiencies and is the most promising material as the air stable inorganic hole extaction layers in perovskite solar cells [24]. Doctor blading, electrodeposition, spin coating, and spray coating have been tried as CuSCN deposition methods [22,25–28]. The solution-based bottom-up processes are more easy to produce; however, most of the solvents in which CuSCN shows high solubility degrade the perovskite layer, so it is the most critical issue associated with these techniques [29]. An inverted device architecture or other deposition routes of CuSCN has been used because of the absence of solvents that readily dissolve CuSCN but not the perovskite [25].

In this work, diethylsulfide was chosen for deposition of CuSCN layers on mesoscopic perovskite solar cells as the hole transport layer. Diethylsulfide is known to have higher solubility compared to dipropylsulfide [29], most common solvent for deposition of CuSCN layers. In addition dipropylsulfide is known to have a polar character and has the potential to damage the perovskite layer [24]. Due to the higher solubility of CuSCN in diethylsulfide, we could succesfully achieve to deposit homogeneous and sufficiently thick CuSCN layers by a simple spin coating technique compared to the unreproducible doctor blading and electroplating techniques employed in previous studies. Effect of CuSCN thickness and morphology of the CuSCN layers were investigated and correlated to the performance of the cells.

CHAPTER 2

LITERATURE SURVEY

The first empirical photovoltaic (PV) cell based on crystalline silicon was established at Bell Laboratories, in 1954 [30]. In 2014, technology of crystalline silicon commands the PV market worldwide with a 60% and 40% market portion for modules with monocrystalline and polycrystalline silicon cells after many decades of progression [31]. The outstanding 10% of the industry was separated between a diversity of other developed and rising photovoltaic technology applications, including amorphous semiconductors, polycrystalline thin films, organics, dye sensitized solar cells (DSSCs) and quantum dot solar cells [32]. Alternative technology progress have to be provided with a desired assembly of high power conversion efficiency (PCE), outstanding stability and lower fabrication costs. Organo metal halide perovskites (OMHPs), with methylammonium lead iodide ($CH_3NH_3PbI_3$ or $MAPbI_3$) are proposed as a prototypic instance that have great potential to satify these provisions and being competitive in the solar cell industry. The historic evolution of perovskite solar cells from DSSCs is shown clearly in Figure 2.1. After many intensive research applications over the world [33-42] perovskite solar cells are corresponding or better than other PV applications with lover fabrication costs, easy device processing, and suggesting the potential to challenge the dominant silicon solar cell technology in the future. Perovskite mentions the crystal structure of calcium titanate ($CaTiO_3$) that was identified by the Gustav Rose and named in honour Lev Porovski [43]. OMHPs are identified with a group of materials and these are formulated AMX_3 , where A represents an organic cation ($CH_3NH_3^+$ or $NH_2CH3NH_2^+$), M represents a divalent metal cation (Pb^{2+} or Sn^{2+}), and X represents a monovalent halide anion (I^-, Br^- or Cl^-) in the area of optoelectronics. Single cyrstal of organometal halide perovskite ($MAPbI_3$) and crystal structure of it is shown in Figure 2.2. At the center of the cube structure, M^{2+} cation is located, eight of A^+ cations are located at the corner of a cubic cage, and

six of octahedrally coordinated X^- species located at the cube's faces. Researchs of OMHP group of materials were started in 1990s due to their superb optoelectronic properties and solution-based processible potential, [44,45–47] but the principle aim of early works was to develop new materials for field effect transistors and organic light-emitting diodes [48,49].
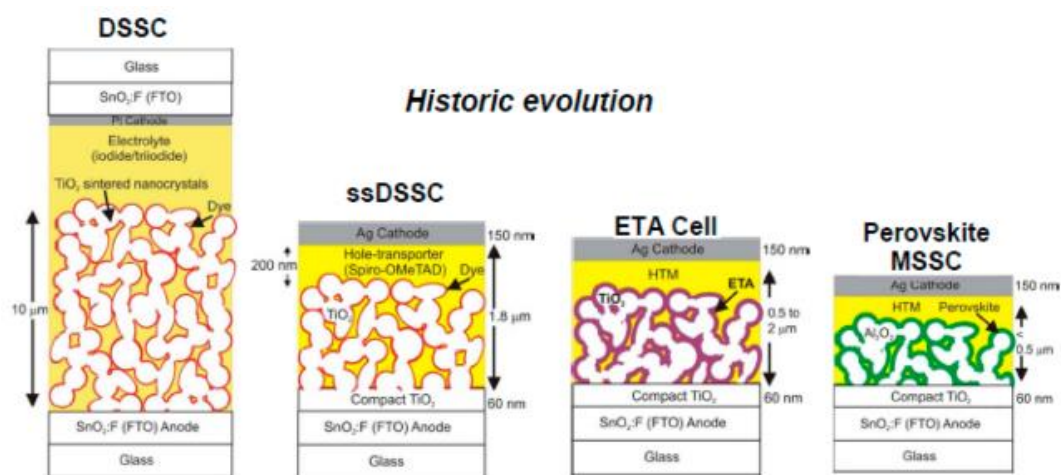
Figure 2.1. Historic developments in the solution based solar technology applications, beginning from the electrolyte based mesoscopic DSSC, the solid state DSSC (ssDSSC), the excessively thin absorber layer (ETA) cell, to the MSSC [50].

The first study of OMHP materials in DSSC as a dye material which is reported with %3 of PCE in 2009 [51]. Because of the poor stability and low efficieny, this OMHP-based solar cell electrolyte containing did not take a high attention. After development of solid state device with 10% PCE in 2012 [52], perovskite had more interest in the industry [53,54]. Since then, the performances of OMHP-based photovoltaic device has rapidly increased, and best reached efficiency of 21% was successed in late 2015 [55]. In PV history, the enhancement has been exceptional and unprecedented. It is attributed to ease of processing, inexpensive fabrication costs, and the superior optoelectronic properties of the materials [36,38,39–42].

4
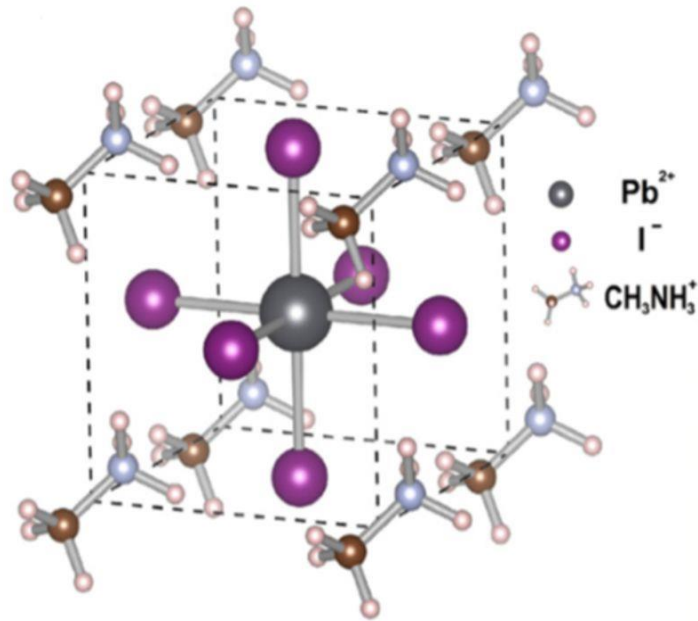
Figure 2.2. Crystal structure of $CH_3NH_3PbI_3$ perovskite [16].

Many of high-quality perovskite thin film fabrication processes are in conformity with large scale, low cost and industrial production techniques [54-56]. These techniques contain vapor-based deposition methods and which are solution operation during process. [57-59]. Due to production strengths and its advantages, perovskite solar cells have potential for the commercialization. DSSC, organic photovoltaics (OPV), and solution processing are favored to study by many scientists and researchers from all around the world. For this reason, perovskite solar cells generation has been developed in a very short time. OMPH materials have many high-grade optoelectronic properties for processing flexibility. $MAPbI_3$ bandgap which is 1.55 eV can change between the range of 1.45 eV and 2.35 eV continuously because of interchanging the halide and organic ions [60,61] . Changeability of the bandgap makes a kind of an ideal situation for single junction based solar cells exposed to the solar irradiance spectra. Methyl ammonium lead iodide ($MAPbI_3$) has high optical absorption coefficient than the other PV materials such as Si, CdTe, $CuGa_xIn_{1-x}S_ySe_{1-y}$ (CIGS), and amorphous Si:H; for this reason to reduce the costs of materials, the thickness of absorber can be reduced to about 300 nm [62,63]. Exciton binding energy of OMHPs is lower when it compares the

5

other PV materials and this low binding energy cause excitation into free charges after light absorption that occur spontaneously [64–66]. Therefore, charge carriers have long diffusion lengths (∼1 μm) and can be freely carried across the 250-300 nm thick perovskite absorber layer without any recombinations. Perovskites has high charge carrier mobility about 10 to 60 cm^2 V^{-1} s^{-1} and long carrier life time (∼100 ns) that prevents the possible recombinations [67–70]. As a result, higher open circuit voltages than 1 V is achieved, because the electronic flaws are slight, and the non-radiative recombination rates are low [71,72].

The perovskite solar cells have extensive useage of area and big impress, but commercialization of these devices has many difficulties to get over. Especially, the longtime stableness of OMHPs is one of the points worth stressing which is not achieved yet. This stability is necessary for fabrication of 30-year lifetime CdTe and Si solar panels that has also a commerical purpose. An unstable situation may cause the current–voltage (J −V) hysteresis during voltage scanning for large-scale production. Besides, the potential impacts to environment of perovskites should be considered, because OMHPs contains Pb ions.

During the evolution of different types of perovskites and device fabrication techniques, the main success and improvement came about in efficiency, however HTM used were bounded by organic compounds, the state-of-the-art 2,20,7,70-tetrakis(N,N-di-p-methoxyphenylamine)-9,90-spirobifluorene (spiro-MeOTAD) [72–74] and other small molecules. pyrene arylamine derivatives [75] and conducting polymers are some examples of these molecules [76-78]. These HTMs are very expensive, especially n-type semiconductors (TiO_2, ZnO) were considered. Therefore, this situation causes the limitation of these materials for further large-scale application. Lately, several inorganic hole transport materials have been studied to apply the device fabrication for developing the stability and reduce the cost of PSCs. Instead of organic HTMs, inorganic p-type semiconductors are likely a clever option, beacuse of their high mobility, ease of synthesis, stability and low costs. Copper iodide (CuI) was just notified in lead halide perovskite-based devices as a hole conductor, showing 6% PCE [79]. Another interesting inorganic p-type semiconductor , which shows good transparency throughout the visible and near

infrared spectrum, is copper thiocyanate (CuSCN). It has high hole mobility and good chemical stability [80–83].

2.1 Device Structures of Perovskite Solar Cells

It is the first application of OMHPs in PV that were used for dye sensitizers in the DSSCs as replacement directly as explained above [51-71]. In typical basic DSSC architecture consists of a several micron thick mesoporous TiO_2 layer, which is penetrated to dye molecules, and coated with dye material and used to collect and conduct the electrons. A liquid electrolyte containing redox couple provide connection in electrodes and it acts as a hole transport layer [84]. The main structure of perovskite solar cells, while the OMHP materials acting simply as a dye replacement, evolved from this structure. Using a solid state material for hole transportation rather than the liquid electrolyte in mesoscopic structure (Figure 2.3-a) increased the interest of perovskites [53,54]. This advance made great interest in PV communities. As a result, planar device structures were developed by the OMHP absorber sandwiched between hole transport material (HTM) and electron transport material (ETM). Two planar device architectures categorized by encounting with the light first which are the conventional n-i-p (Figure 2.3-b) or the inverted p-i-n (Figure 2.3-c) structures. Recently, a mesoscopic p-i-n structure of cells also has been developed [85,86]. Charge transporting materials which are ETM and HTM and contact materials (cathode and anode) are chosen by different processing of the device architectures.

2.1.1 Conventional n-i-p Architecture

The mesoporous n-i-p architecture is still the most widely used one to construct high efficient cells and the original structure of the perovskite photovoltaic devices. This architecture of perovskite solar cells, which is showed in Figure 2.3-a, consists of a

transparent conducting oxide (TCO) generally fluorine doped tin oxide (FTO) coated substrate as cathode, a thickness of 50 to 70 nm compact electron transport layer (ETL) (typically TiO_2), a thickness of 150 to 300 nm mesoporous metal oxide material (mp-Al_2O_3 or mp-TiO_2) which is filled with perovskite crystals, followed with an up to 300-nm thick perovskite excitation layer, a 150 to 200 nm thick layer of polymeric materials mostly 2,2',7,7'-tetrakis(N,N-di-p-methoxyphenylamine)-9,9'-spirobifluorene (spiro-MeOTAD), which is a hole transport material, and about 50 to 100 nm of a metal contact material as an anode (Au or Ag).
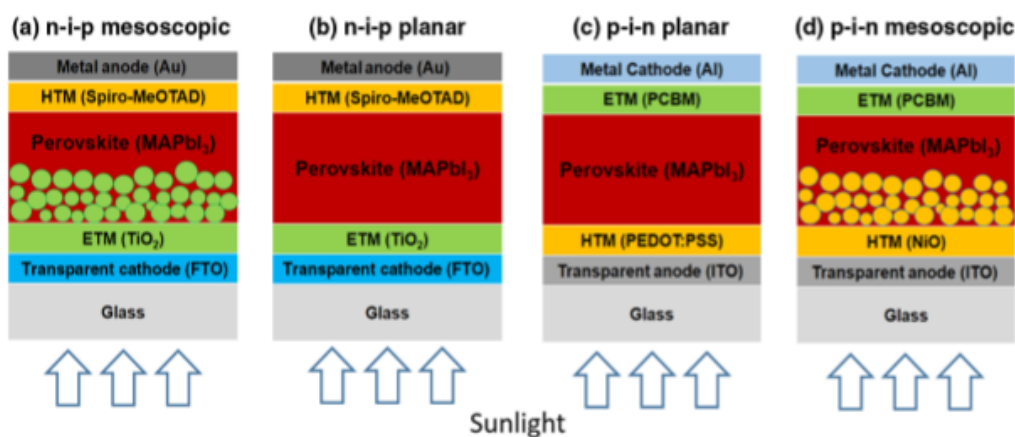
Figure 2.3. Schematic diagrams of perovskite solar cells (a) n-i-p mesoscopic, (b) n-i-p planar, (c) p-i-n planar, and (d) p-i-n mesoscopic structures [169].

The assignment of mesoscopic layer in this architecture is decreasing the carrier transport distance and enhancing charge collection. The mesoscopic layer is enhancing the absorption of photons and also avoiding direct current leakage between the two selective contacts due to light scattering in structure. So, the main mesoporous perovskite cells employed a thick porous layer (>500 nm) for absorbing the incident light effectively [53-71, 84-89]. But, an important quantity of material exhibits disordered and amorphous phases because of the grain growth of the perovskites is confined by the pores in the structure [90]. This causes a relatively decrease in short circuit current density (J_{SC}) and open circuit voltage (V_{OC}) [91].

8

When thinning the mesoporous TiO_2 layer about 150 or 200 nm levels, crystallinity in the perovskite absorber is enhanced and the device efficiency improves. Additionally, the pore filling fraction and morphology of the perovskites is critically dependent with the thickness of mp-TiO_2 [92,93]. The pore filling fraction is increased and a perovskite capping layer forms on top of the porous structure with the porous layer is thinned to lower than 350 nm thickness. Pore filling formation of perovskite capping layer is important for high charge transporting rates and high charge collection efficiencies at the region of perovskite TiO_2 interface. Due to the conduction and valence energy band positions, possible recombination pathways between holes in HTM and electrons in TiO_2 are prevented when charges are separated once [92]. Accordingly, the mesoporous n-i-p structure of perovskites is the most favoured architecture in the literature. The last recorded cell efficieny was 20.2% in the mesoscopic structure.

The planar n-i-p structure is showed in Figure 2.3-b and it represents the natural evolution of the mesoporous structure. Due to hole extraction at the hole transport layer interfaces is considerably more efficient than electron extraction at the electron transport material interfaces, it is critical that ETM was concieved with larger area initially for high-efficiency perovskite solar cells [94]. However, high efficiencies in device can be achieved without a mesoporous layer by finely optimizing the formation of the perovskite light absorber layer, and the interfaces between the perovskite, charge transporting layers, and contact materials [95]. To date, best efficiency value reached in planar n-i-p device structure was 19.3%, in which it was conducted by the optimization of electron transporting layer TiO_2 and ITO contact layer interface [95]. Although perovskite cells with the planar n-i-p configuration usually demostrate increased V_{OC} and J_{SC} values related to a comperative mesoporous device refined with the same materials and approach, the devices with planar structure usually shows more harsh J-V curves. Hence, n-i-p configurated devices generally contains a thin mesoscopic layer about 150 nm that capped and filled with the perovskite material [96].

9

2.1.2 Inverted p-i-n Device Architecture

The device is designed and fabricated in the p-i-n structure when the HTM layer is deposited first on the conducting substrate as shown in Figure 2.3-c. This type of perovskite devices are built on a 40 to 70 nm thickness of p-type polymeric conducting layer such as poly (3,4-ethylenedioxythiophene) poly (styrene-sulfonate) (PEDOT:PSS) as a hole transporting material, which is deposited on transparent conducting ITO coated substrates. After deposition of intrinsic perovskite thin film about 300-nm thick, the cell is accomplished by a 20 to 50 nm organic [6,6]-phenyl C61-butyric acid methyl ester (PCBM) as a hole blocking layer and a metal cathode contact material (Al or Au). A fullerene (C_{60}) and perovskite acceptor-donor pair is applied in earyl device design, which is typical in organic photovoltaics (OPVs) [97]. OVP researchers moved into the field of perovskites easily due to the similarity in structures. When the field has improved, the planar perovskite layer sandwiched among two contrast organic charge transport materials and the organic acceptor has been excluded in favor of an ETM layer [98]. Recently, the use of more advanced material preparation methods provided the improvement of the p-i-n structure efficiencies and a best efficiency of 18.9% was achieved in planar p-i-n structure [99].

Additional generation of the p-i-n architecture has enlarged the charge selective contact material choices from organic to non-organic materials. For instance, NiO layers have been used as the hole selective and ZnO/TiO_2 layers have been used for the electron transport layer recently that cause the perovskite solar cell exactly free from its organic counterparts [100,101]. To fabricate high efficiency perovskite solar cells in large area, different inorganic charge transport layers such as NiMgLiO and $TiNbO_2$ have also been used. This is an important step for the commercialization of perovskites. [100] Employing inorganic oxide p-type hole transport materials permits the production of mesoporous p-i-n device architecture shown in Figure 2.3-d, in which compact NiO / mesoporous-Al_2O_3 or compact-NiO / mesoporous-NiO are used as the HTM [85,86]. The best results were obtained with 17.3% efficiency in NiO hole transport material included mesoporous p-i-n device structure [102].

10

2.2 Deposition Methods of Perovskite Thin Film

The film quality of the absorber material determines mainly the device performance of most thin film based solar cells. The morphology, phase purity, crystallinity and uniformity of perovskite films are significant for high-performance PV devices. Crystallization, interface properties, and composition of perovskite films are needed to be studied for the quality criteria. Deposition of the films contains critical issues as processing condition, procursor composition and additive control. These can affect the quality and crystallization of perovskite films.

2.2.1 Single-Step Solution Deposition Method

For perovskite thin film deposition, single-step solution deposition process is commonly used because of low costs and ease of processing. In order to prepare precursor solution, lead halides and organic halides such as methylammonium iodide (MAI) are generally dissolved in dimethyl sulfoxide (DMSO), gamma-butyrolactone (GBL), or dimethylformamide (DMF). The prepared precursor solution is spinned on the substrate followed by a post deposition heating at 150 °C or 100°C for perovskite film generation. As the perovskite allowed composition variations [93], high-efficient perovskite cells can be produced through a wide range precursor ratios of MAI and PbI$_2$ from MAI-poor (1:2) [66] to MAI-rich (3:1) compositions [86]. But, it is crutial to proper times and processing temperatures based on different precursor compositions to reach the desired phase, morphology and crystallinity of the perovskite films [83,93,94]. Along with the choice of processing temperatures and precursor composition, material of substrate, the environment (humidity and oxygen levels) , and deposition parameters have to be controlled also. The best efficient solid state device fabricated with the single step solution method presented 9.7% efficiency [95]. The reached best efficiency increased to 19.7% using single-step solution deposition method after developing advanced engineering techniques [97].

The other solution based perovskite deposition techniques are doctor-blade, spray coating, inkjet printing and slot-die printing [98-101]. In addition to spin coating, these techniques have also been studied to produce perovskite solar cells. These techniques show the potential for roll-to-roll large scale fabrication of perovskite solar cells. Still, present devices that produced by these methods have lower efficiencies than the spin coated devices due to the complicacies related with compositional uniformity and the film morphology (Figure 2.4-a).

2.2.2 Two-Step Solution Deposition

Preparing OMHPs with the two-step solution deposition method was introduced by Mitzi et al. in 1998 firstly [102]. Beyond this spearheading work, Gratzel et al. improved a two step sequential deposition technique (Figure 2.4-b) to fabricate perovskite devices, which was reported with efficiencies higher than 15%. In a basic two step solution deposition procedure, $APbI_2$ seed layer is deposited first and then transformed to $MAPbI_3$ by dipping the $APbI_2$ coated substrate into an MAI/isopropanol solution [56]. Spin coating of MAI has also been use to embed MAI molecules into the PbI_2 network [95]. Produced perovskite layers with two step sequential deposition process gives denser and more uniform films when compared with the single step solution process [103]. The process can be well controlled and, eventually, has been extensively used to produce high-efficiency cells [56,84,104,105].

The two-step solution process ensures a reproducable way to produce high-quality perovskite films. The perovskite grain size can be controlled with changing the MAI solution concentration [95]. However, the trade-off between perovskite surface smoothness and grain size is one of the disadvantages of the two-step solution preparation technique. Thin films involved large grains of perovskites typically present lower surface coverage, and it limits the performance of perovskite devices. Unsatisfied perovskite conversion is the other issue with two-step solution deposition method. When the film dipped into solution PbI_2 to MAI

12

conversion rapidly occurs because the heavy metal halide coated structure is prone to interaction with small molecules [106]. Thereby, on the surface of PbI_2 a dense perovskite capping layer usually occurs and inhibits the diffusion of MAI molecules to the underlying layer, that is causing non complete perovskite conversion. After overcoming these costraints by new engineering techniques, the efficiency of champion cell has been increased to 20.2% using the two-step solution deposition method [84].
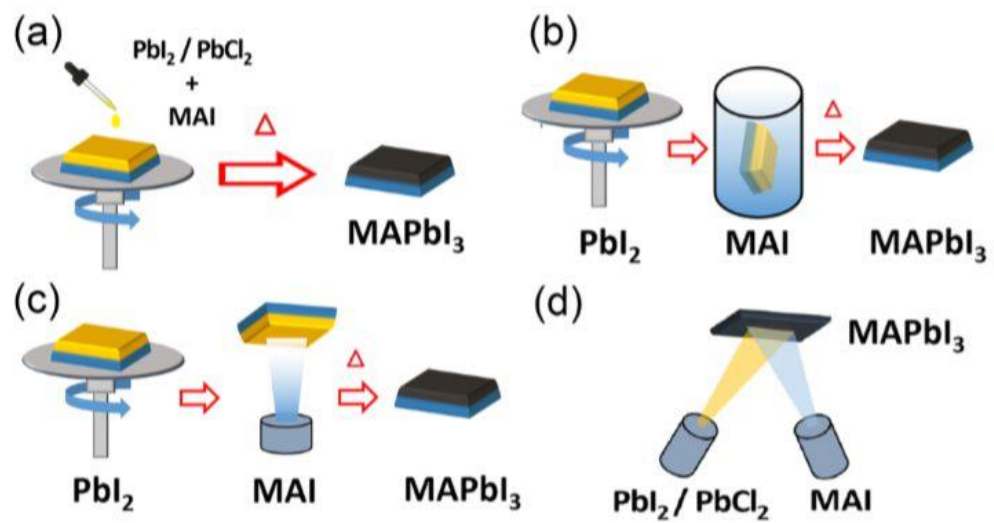
Figure 2.4. Production techniques for perovskite thin films, (a) single-step solution deposition, (b) two-step solution deposition, (c) two-step hybrid deposition, and (d) thermal vapor deposition [169].

2.2.3 Vapor Assisted Solution Deposition Process

In one alteration to the two-step solution deposition technique, MAI is produced via vapor deposition method instead via solution processing (Figure 2.4-c) [58]. This deposition technique permits better grain size and morphology control through solid-gas interaction and effectively hinders film delamination which can happen

13

during solid-liquid interaction. Deposited perovskite thin layers with this process present large grain size, full conversion and uniform surface coverage. However, this method has some restrictions, because the solid and gas reaction typically needed tens of hours for the full perovskite conversion, and devices fabricated by this deposition technique have reached from 10% to only 12% efficiency [58,107].

2.2.4 Thermal Vapor Deposition

For producing high quality semiconductor thin layers with uniform composition and thickness, vapor phase deposition is commonly preferred. The first uses of the thermal vapor deposition of OMHP thin films was demostrated by Mitzi et al. in 1999 [45]. The first planar heterojunction $MAPI_{3-x}Cl_x$ perovskite solar cell was produced by Snaith et al. after alteration of the method for dual source thermal evaporation (Figure 2.4-d) with an efficiency of 15% [57]. Chemical vapor deposition [108] and sequential layer by layer vacuum sublimation [59] have also been developed as an example of vapor-base deposition method.

The perovskite films are extremely uniform and pin-hole free which was produced by thermal vapor deposition technique. Vapor-deposited perovskite films can constantly coat PEDOT:PSS and TiO_2 layers when compared with perovskite films produced by solution processing because of the surface coverage [57,88,109]. However, the vapor deposition needs exact control of temperatures during deposition because both the products and the procursor sources have low thermal stability. Thus, high-efficiency devices produced using this method have been reported by only a few research groups [57,59,88,109,110].

2.3 Working Principle of Perovskite Solar Cells

The electronic and optical properties of perovskite materials have been investigated entirely in recent ten years [111-114]. Working mechanism of perovskite solar cells

can be described using equations occurred in cell as follows (Figure.2.5). Sunlight is absorbed by perovskite material and electron-hole pairs are produced in this material, which can possibly spread towards the exciton formation after thermalization of carriers. Then, two possible primary reactions can occur for charge separation: injection of holes through hole-transport material (HTM) (Eq.[2.1-a]) and/or photogenerated electron injection into TiO_2 nanoparticles (Eq.[2.2-a]) [115,116]. However, that first occurred injection process is a hole or electron injection, and in the latter case, whether electron injection into and transfer within the oxide mesoscopic film (Eq.[2.1-b]) is playing role, remain unclear. The exact role of mesoporous titanium dioxide in efficient perovskite solar cells has actually not been determined explicitly yet. For electron injection from mixed halide $CH_3NH_3PbI_2$ into TiO_2 evidence has been found [117,118], and the same material has also been studied to yield effective photovoltaic conversion once dispersed on an alumina structure, where no metal oxide material sensitization can be referred and in which electron injection is not energetically performable [117].
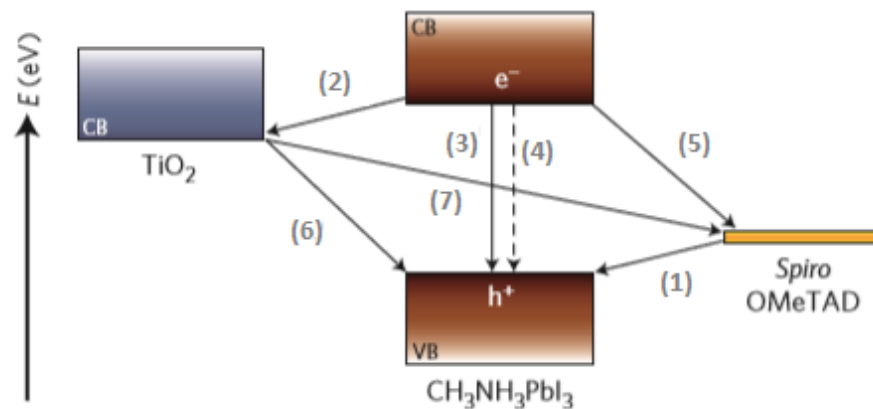
Figure 2.5. Schematic diagram of energy levels included interlayer energy transfer reactions in perovskite solar cells.

Hole injection as the primary charge separation step:

$$(e^-...h^+)_{perovskite} \rightarrow h^+(HTM) + e^-(perovskite)$$

Eq.[2.1-a]

$$h^+(perovskite) \rightarrow h^+(HTM)$$
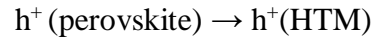
Eq.[2.1-b]

Electron injection as the primary charge separation step:

$$(e^-...h^+)_{perovskite} \rightarrow e_{cb}^-(TiO_2) + h^+(perovskite)$$

Eq.[2.2-a]

$$e^-(perovskite) \rightarrow e_{cb}^-(TiO_2)$$
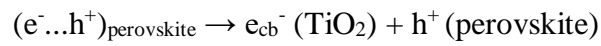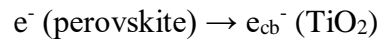
Eq.[2.2-b]

Exciton destruction:

$$(e^-...h^+)_{perovskite} \rightarrow h\upsilon'$$

Eq.[2.3]

$$(e^-...h^+)_{perovskite} \rightarrow \nabla$$
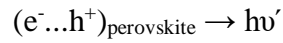
Eq.[2.4]

Back charge transfer at the HTM surface :

$$h^+(HTM) + e^-(perovskite) \rightarrow \nabla$$

Eq.[2.5]

16
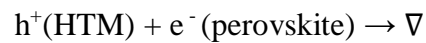
Back electron transfer at the TiO_2 surface:

$$e_{cb}^- (TiO_2) + h^+ (perovskite) \rightarrow \nabla$$
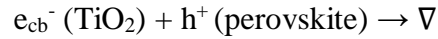
<div align="right">Eq.[2.6]</div>

Recombination of charge at the HTM/TiO_2 interface:

$$e_{cb}^- (TiO_2) + h^+ (HTM) \rightarrow \nabla$$
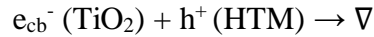
<div align="right">Eq.[2.7]</div>

Exciton destruction, causing photoluminescence (Eq.[2.3]) or non-radiative recombination (Eq.[2.4]), as well as recombination of the charge carriers at the interfaces of layers (Eq.[2.4, 2.5, 2.6 and 2.7]) are undesired reactions. Possible recombinations are represented by ∇ in the given equations. Thus, the kinetics of these undesired processes are expected to control the overall photovoltaic conversion efficiency of the system.

2.4 Hole Transporting Materials in Perovskite Solar Cells

Hole transporting materials (HTM) are available for many objectives in perovskite solar cells :

i. It blocks the electron transfer to anode, so it acts as a physical energetic barrier between anode material and perovskite absorber layer [119].

ii. It enhances the efficiency of hole transfer [120].

iii. It affects the open circuit voltage (V_{oc}) by identifying the separation of the quasi Fermi-energy levels of the perovskite [121-124].

iv. It prevents the degradation at the perovskite-metal contact (Au) interface that would occur in the absence of a HTM [125,126].

Actually, viewing of convenient hole transporting materials (HTMs) and a perovskite cause a V_{oc} as high as 1.5-1.61 V in perovskite solar cells [127,128]. When a cell constructed using only a perovskite layer is compared with a cell constructed using perovskite and HTM layers, HTM containing cells showed an improvement of surface coverage and annihilation of charge recombination by fully separating the top contact from transport layers evoking enhanced performance. The stability of cells has been shown to increase with the choice of convenient HTM, except profits of photo current efficiency. An inorganic HTM layer NiO_x can be given as an example for this phenomenon. NiO_x in inverted PSCs not only proved a higher 16% PCE but also showed stable performance of 90% for over 2 months of air storage [129]. PEDOT:PSS that the champion cell uses as HTM layer in inverted PSCs is sensitive to humidity, and its acidic nature leading to degradation on conducting substrates. Additionally, the high cost of fabrication should be considered when commercialization is the point [130]. Admittedly, it is no doubt that HTM is the most expensive part in PSCs.

Many HTM layers have been studied up to now, but P3HT and Spiro-OMeTAD are giving by far the best cells with regard to the performance with higher efficiencies than 15%. Although they give the best efficient performance,

i. These materials are often qualified by poor hole mobility in their main form.

ii. These materials upon addition of any dopants become sensitive to humidity. Stable performance of PSCs is often prevented by this humidity sensitiveness of these materials.

iii. These materials are expensive (1 g of Spiro-OMeTAD costs 500 $).

Because of these hard conditions about the hole transport layers used in perovskite cells, commercialization of these devices have several constraints. However, device performance has become a necessity in recent devices. These conditions bring into the usage of p-type inorganic materials as hole transport layer that have already demostrated in the DSSCs and quantum dot solar cells due to their higher band gap and high conductivity [131-133]. Additionaly, many studies have demonstrated that

spiroOMeTAD based hole conductors underperformed these inorganic counterparts in dye-sensitized solar cells [134,135]. Operating some inorganic p-type materials in PSCs will both provide to reach higher PCEs and especially accomplish in long term stability and cost-effective PSCs. Such inorganic p-type materials are CuSCN, Cu_2O, NiO, CuI, MoO_3, GO (graphene oxide), and lead sulfide quantum dots (PbS QDs), studied as HTM in PSCs (Figure 2.6). Different HTMs used in perovskite solar devices indicating their efficiencies are shown in Table 2.1.
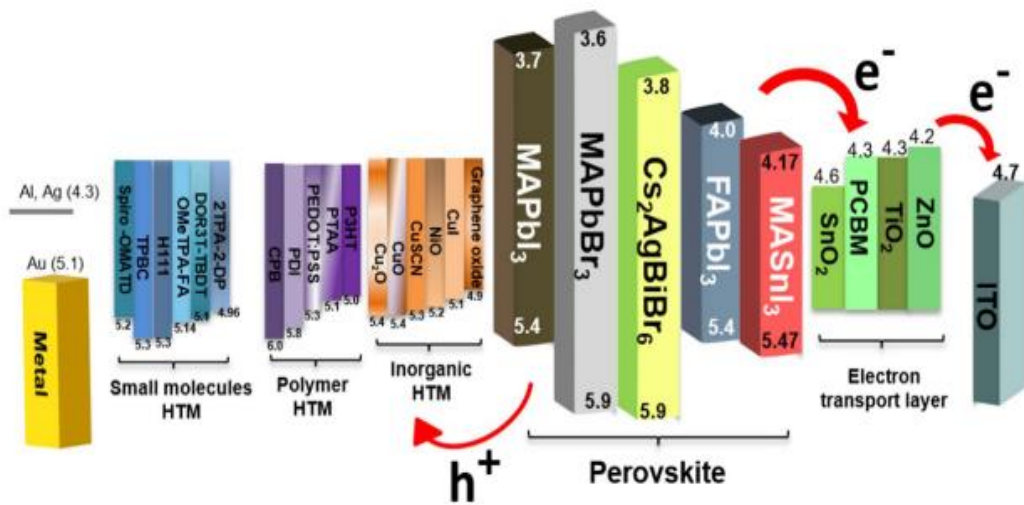
Figure 2.6. Energy level diagram of several common hole transport matrials together with bromide and iodide based halide-perovskites. It is significant to note that the given energy levels are those of isolated materials and that upon formation of the multilayer device, changes in the energy scheme and alignment may occur due to interfacial dipoles, band bending, trap states and impurities [136].

19

Table 2.1. Several hole transport materials employed in perovskite solar cells.

HTM	Hole Mobility (cm^2 V^{-1} s^{-1})	Cost/g ($)	Perovskite Material	Perovskite Deposition	Device Structure	PCE (%)	V_{oc} (V)	Ref.
Spiro-OMeTAD	10^{-3}-10^{-4}	500	$CH_3NH_3PbI_3$	OSSD	Mesoscopic	19.71	1.08	[137]
FDT	-	60	$FAPbI_3$/$MAPbBr_3$	OSSD	Mesoscopic	20.2	1.14	[138]
P3HT	<0.1	400	$CH_3NH_3PbI_3$	OSSD	Meso-superstructure	15.3	1.02	[139]
PTAA	10^{-2}-10^{-3}	2500	$(FAPbI_3)_{1-x}$/$(MAPbBr_3)_x$	TSSD	Mesoscopic	20.2	1.06	[140]
PEDOT:PSS	10^{-2}-10^{-3}	200	$CH_3NH_3PbI_3$	OSSD	Inverted-planar	18.1	1.1	[141]
CuI	9.3	10-15	$CH_3NH_3PbI_3$	GSC	Inverted-planar	13.58	1.04	[142]
CuSCN	25	2	$CH_3NH_3PbI_3$	OSSD	Inverted-planar	16.6	1.00	[143]
NiO	0.141	10-15	$CH_3NH_3PbI_3$	SET	Inverted-planar	17.3	1.06	[144]
Cu_2O	100	2-12.5	$CH_3NH_3PbI_3$	OSSD	Inverted-planar	16.52	1.07	[145]
GO	-	300	$CH_3NH_3PbI_3$	SD	Mesoscopic	15.1	1.04	[146]

OSSD: One step spin coating deposition.

SD: Sequential deposition.

GSC: Gas solid crystallization process.

SET: solvent engineering technique.

TSSD: Two step spin coating deposition.

FDT: 2,7-bis(4-methoxyphenyl)amino) spiro[cyclopenta [2,1-b:3,4-b]dithiophene-4,9-fluorene.

PMMA: poly(methyl methacrylate)

2.4.1   Copper (I) Thiocyanide (CuSCN) As a Hole Transport Material

Copper (I) thiocyanide (CuSCN) is a wide bandgap (>3.4 eV) [147,148], and inorganic molecular semiconductor material that associates efficient hole-extraction (p-type) characteristics with charming mechanical properties and high optical tranparency [148-150]. CuSCN has hexagonal structure which is shown in Figure 2.7. In many novel optoelectronic devices [151], including organic photovoltaic cells [153,154], integrated circuits and thin film transistors [148,150,152], hybrid perovskite cells [155-157], and light emitting diodes [158,159] CuSCN has been demostated as a hole transport material. A wide range of solution prosessing methods could be used for CuSCN deposition at low temperature, which include ink-jet printing [160,161], spin coating [148,152,153], doctor blading [162], electrochemical deposition [165–167], and spray coating [163,164]. The versatility of CuSCN deposition processes allows its combination as inexpensive and applicable on temperature sensitive substrates [168].

CuSCN is a promising candidate to traditional organic or inorganic hole transport materials due to these physical attributes combined with its commercial availability and low cost.
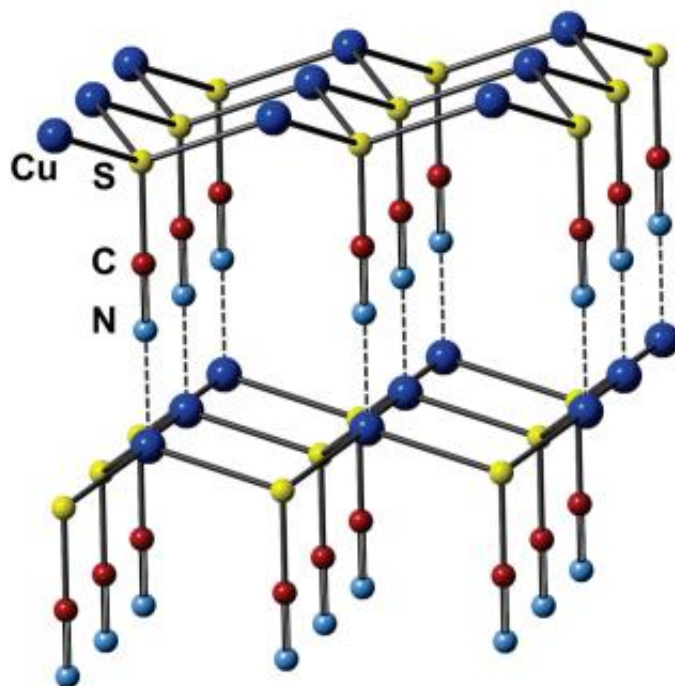
Figure 2.7. 3x3x1 supercell of β-CuSCN hexagonal structure [147].

CuSCN remains respectable HTM in PSCs due to its higher mobility than Spiro-OMeTAD which is around values of 0.01-0.1 cm^{-2} V^{-1} s^{-1}, high chemical stability and good transparency in the infrared and visible regions [166,170,171]. 6.4% PCE with CuSCN in planar structure (FTO/TiO$_2$/ CH$_3$NH$_3$PbI$_{3-x}$Cl$_x$/CuSCN/Au) with 0.62 of FF (fill factor) and 0.72 of V$_{oc}$ is achieved by Chavhan et al. They discussed that PSCs with CuSCN has lower V$_{oc}$ because of lower diffusion length of CuSCN than its actual film thicknesses compared to Spiro-OMeTAD counterpart [172]. The role of CuSCN as hole transport materials in PSCs verified by Ito et al. [173] with comparison of devices as CuSCN included and free. They attained an enhancement in PCE from 1.35% which is HTM free to 1.82% by using CuSCN as an HTM in the following structure (FTO/TiO$_2$/thin CH$_3$NH$_3$PbI$_{3-x}$Cl$_x$/CuSCN/Au). By increasing CH$_3$NH$_3$PbI$_3$ penetration into TiO$_2$ pores using hot air during spinning, a

further enhancement in PCE has been successed which is 4.85%. In another study [162], the same group demonstrated the use of Sb_2S_3 layer between $CH_3NH_3PbI_3$ and TiO_2, and obtained results showed that the added Sb_2S_3 layer not only increased PCE to 5.24%, but also enhanced the device stability under light exposure without cladding. However, a less reactive surface of Sb_2S_3 when compared to TiO_2 that provides enhancement in stability, could react with perovskite and ultimatelly causing its crystal decomposition [175,176]. A 12.4% of PCE is achieved by Qin et al. in mesoscopic architecture of PSCs ($FTO/TiO_2/CH_3NH_3PbI_3/CuSCN/Au$). To avoid direct contact between CuSCN and TiO_2 and to reach thickness of over 200 nm layer, two-step deposition technique was used in this study for perovskite layer deposition. CuSCN layer was also produced by doctor blading deposition at 65 ºC, which is suitable for mass production. J_{sc} and V_{oc} outputs of CuSCN included devices has enhanced 65% and 9%, respectively compared to HTM free structure. After inspiring progress in mesoporous structure, researchers studied CuSCN in following inverted planar structure ($FTO/CuSCN/CH_3NH_3PbI_{3-x}Cl_x/PCBM/Ag$) [178]. Thinner CuSCN layers have low shunt resistance and for thicker layers series resistance is higher. Therefore, the PCE was restricted to 3.8% although CuSCN/FTO interface indicated >90% PL quenching efficiency (Figure 2.8). Further studies in planar heterojunction devices were concentrated on the thickness of CuSCN layer tuning.

Ye et al. reported the highest PCE (16.6%) in inverted planar PSCs of ITO / CuSCN / $CH_3NH_3PbI_3$ / C_{60} / BCP / Ag structure. For the deposition of CuSCN layer, electrodeposition technique was chosen due to lower contact resistance between CuSCN and $CH_3NH_3PbI_3$ layer and a smaller surface roughness. The perovskite layer was also deposited by drop casting assisted one step spin coating method for reaching higher surface coverage. These devices have shown higher FF and V_{oc} values compared to devices produced by a typical sequential deposition method for perovskite layer. It is clearly shown that production methods of perovskite and HTM layers have importance in the performance of these devices. A thin and dense HTM layer leads to perfect transmittance in the visible region of light spectrum and an effective hole extract at the interface of HTM and perovskite. Furthermore, surface

relaxation and surface roughness of perovskite influence the performance of devices. Smoother perovskite layer might lower the costs of PSCs as thinner HTM coverage is required when compared to rough films. CuSCN included perovskite devices with device structures and performances were tabulated in Table 2.2.
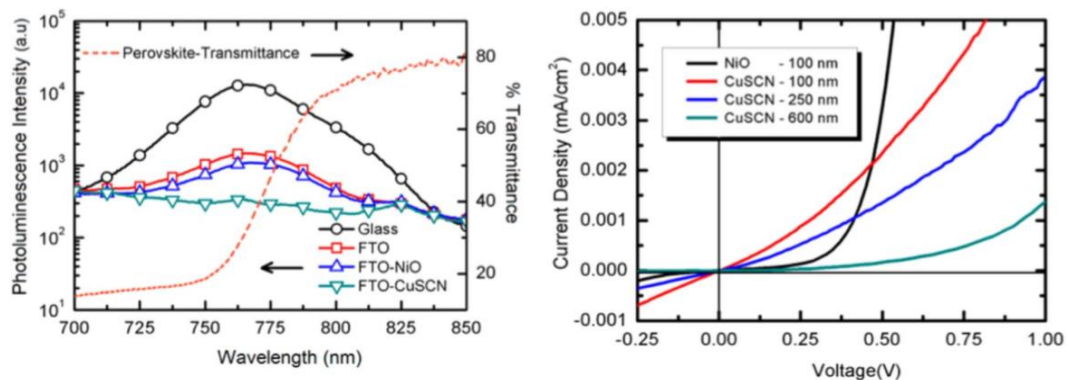
Figure 2.8. (a) Comparison of photoluminescence (PL) intensity spectras of CH₃NH₃PbI₃₋ₓClₓ on (black) glass, (red) FTO, (blue) FTO/NiO, and (green) FTO/CuSCN. Maximum charge extinction is demostrated for perovskite on FTO/CuSCN. **(b)** I−V curves of CuSCN and NiO included PSCs [178].

Table 2.2. Photovoltaic performance and device structures of CuSCN employed as a hole transporting layer in perovskite solar cells.

Device Configuration	Perovskite Deposition Method	Photovoltaic Parameters				Ref.
		V_{oc} (V)	J_{sc} (mA cm^{-2})	FF	PCE (%)	
CL/mp TiO$_2$/CH$_3$NH$_3$PbI$_3$/CuSCN/Au	OSSD	0.63	14.5	0.53	4.85	[173]
CL/mpTiO$_2$/Sb$_2$S$_3$/CH$_3$NH$_3$PbI$_3$/CuSCN/Au	OSSD	0.57	17.23	0.52	5.12	[174]
CL/CH$_3$NH$_3$PbI$_{3-x}$Cl$_x$/CuSCN/Au	OSSD	0.72	14.4	0.61	6.4	[172]
CL/mes-TiO$_2$/CH$_3$NH$_3$PbI$_3$/CuSCN/Au	SD	1.01	19.7	0.62	12.4	[177]
CuSCN/CH$_3$NH$_3$PbI$_3$/C60/BCP/Ag	SD	0.92	21.4	0.68	13.4	[143]
CuSCN/CH$_3$NH$_3$PbI$_3$/C60/BCP/Ag	OSSD	1.00	21.9	0.75	16.6	[143]

CHAPTER 3

EXPERIMENTAL

CuSCN as a hole transport layer included perovskite solar devices were produced during this thesis study. First of all, the advantages and novelty of CuSCN usage in perovskite solar cells were discussed. Then, in order to construct perovskite solar devices, flourine doped tin oxide (FTO) coated glass substrates (20 mmx15 mm, Solaronix 22-7) were used. The layers of cell were constructed on FTO coated glass substrates, respectively. Spin coater used to deposit layers is shown in Figure 3.1. Experimental procedures of cell preparation can be clarified based on the preparation of all layers:

1. Thin film blocking layer preparation
2. Mesoporous layer preparation
3. Perovskite layer deposition
4. CuSCN hole transport layer preparation

After successful preparation of perovskite solar cells, characterizations were performed by using simulated AM 1.5 light. Characterizations of the layers include X-Ray diffraction, Scanning Electron Microscopy, XPS analysis , UPS analysis and UV-Visible measurements.

All chemicals which were used for cell fabrication in this work such as N,N-dimethylformamide (DMF), lead iodide (PbI_2), methylammonium iodide (MAI), diethylsulfide, diethyl ether anhydrous, dimethyl sulfoxide (DMSO) and copper thiocyanate (CuSCN) were purchased from Sigma-Aldrich. All chemicals were used as received without further purification.

3.1   Cleaning and Preparation of Substrates

Firstly, flourine doped tin oxide (FTO) coated glass substrates (20 mmx15 mm, Solaronix 22-7) were wet-etched with zinc powder and hydrochloric acid. The substrates were masked with vacuum tape for desired surface area. Zinc powder and hydrochloric acid reaction etch FTO layer on glass substrate about 5 minutes properly and the reaction stops with deionized (DI) water. After etching of substrates, cleaning is essential for good adhesion of layers. Etched FTO coated glass substrates were cleaned in detergent solution in order to remove dust and organic contaminants with ultrasonic treatment for several minutes. After detergent solution cleaning, substrates were cleaned again in DI water medium using ulrasonication. Residual organic contaminations were further removed by treating the substrates with acetone in ultrasonic bath for 20 minutes and DI water again. The substrates were finally cleaned with isopropanol in ultrasonic bath for 20 minutes and kept in isopropanol solution until the fabrication of devices.

3.2   Thin Film Blocking Layer Deposition

TiO_2 blocking layer was deposited on clean FTO substrates by magnetron sputtering (Leybold, Uniwex 300) from a 3 inch TiO_2 sputtering target. Before this deposition process, substrates attached on the holder of sputter system using vacuum tape at two corners of substrates. The deposition process was performed in high vacuum. Deposition process was started about $2x10^{-6}$ mbar levels and desired thicknesses of TiO_2 material (25 nm, 50 nm, 75 nm, 100 nm) were sputtered at 250 W RF power after 100 nm free sputtering of TiO_2.

3.3   Mesoporous TiO_2 Layer Deposition

Mesoporous TiO_2 layers were deposited on the blocking layers (BL) by spin coating a solution of TiO_2 nanoparticle paste diluted with ethanol with a ratio of 1:3. For the preparation of TiO_2 paste in this work, firstly metal oxide nanoparticles were

dispersed in ethyl cellulose (Aldrich) as the binder and terpineol (anhydrous, Fluka) as the carrier. Synthesized nanopowders were grinded in a mortar and ethanol was added slowly to the mortar. An amount of 30 ml ethanol was added to mortar drop by drop under stable grinding, in order to prevent formation of large aggregates. After preparation of the homogeneous colloid, it was transferred to a beaker using excess ethanol and finalized to approximately 100 ml. This colloid was ultrasonically treated for 10 minutes with an ultrasonic titanium horn. The ultrasonication was followed by stirring the colloid using a magnetic stirrer and repeating the ultrasonication again. Terpineol was added under stirring to this dispersion of the particles and the ultrasonication was repeated. Meanwhile a solution of ethyl cellulose (10% wt.) and ethanol was prepared by stirring the solution for about 30 minutes. This prepared solution was added to the terpineol-ethanol mixture when stirring and final solution was mixed for 1 minute and ultrasonicated for 15 minutes. The final solution contains 10% ethyl cellulose, 20% metal oxide powder and 70% terpineol and excess ethanol. This excess ethanol was evaporated in a laboratory rotary evaporator at 40°C and spinning for about 6-7 hours until evaporation of ethanol is completed. Resulting mixture is a highly viscous paste containing the desired metal oxide nanopowders. This mixture was diluted by ethanol with a ratio of 1:3 to prepare a spin coating precursor solution. Spin coating was conducted at 2000 rpm for 20 s. TiO$_2$ layers with different thicknesses were achieved by repeating the coating procedure after drying. Drying was performed at 125°C for 5 min and substrates were fired at 500°C for 15 min. After cooling down, TiO$_2$ films were subjected to TiCl$_4$ treatment by immersing the substrates into 0.2 mM TiCl$_4$ aqueous solution at 90°C for 10 min.

Figure 3.1. Spin coater used for the deposition of layers.

3.4   Deposition of Perovskite Layer

For deposition of perovskite layers, adduct method was followed [179]. Adduct method for perovskite layer deposition is showed in Figure 3.2. A 40 wt% perovskite precursor was prepared in DMF including PbI_2, MAI and DMSO with a molar ratio of 1:1:1. This precursor was spin coated on TiO_2 coated substrates at 4000 rpm for 30 s. During spinning, 0.2 ml diethly ether was poured at once on the spinning substrate at the fifth second. Transparent films were crystallized at $100^{\circ}C$ for 5 min and shiny black films were obtained.

Figure 3.2. Schematic illustration of perovskite deposition (Adduct method) [180].

3.5 CuSCN Layer Deposition and Completing Cells

For deposition of CuSCN layers, diethylsulfide was chosen as the solvent where CuSCN is known to have higher solubility compared to dipropylsulfide which is most common solvent for deposition of CuSCN layers. A stock solution of 50 mg/ml CuSCN solution in diethylsulfide was prepared. CuSCN layers on perovskite surface with different thicknesses were achieved by diluting this solution. Spin coating was performed at 2000 rpm for 30 s. Films were dried at room temperature and 100 nm gold was evaporated on the finished cells by e-beam evaporation (Leybold Uniwex 350) at 5×10^{-6} mbar. Completed cell is shown in Figure 3.3. Active area of the cells were set to 0.07 cm^2.
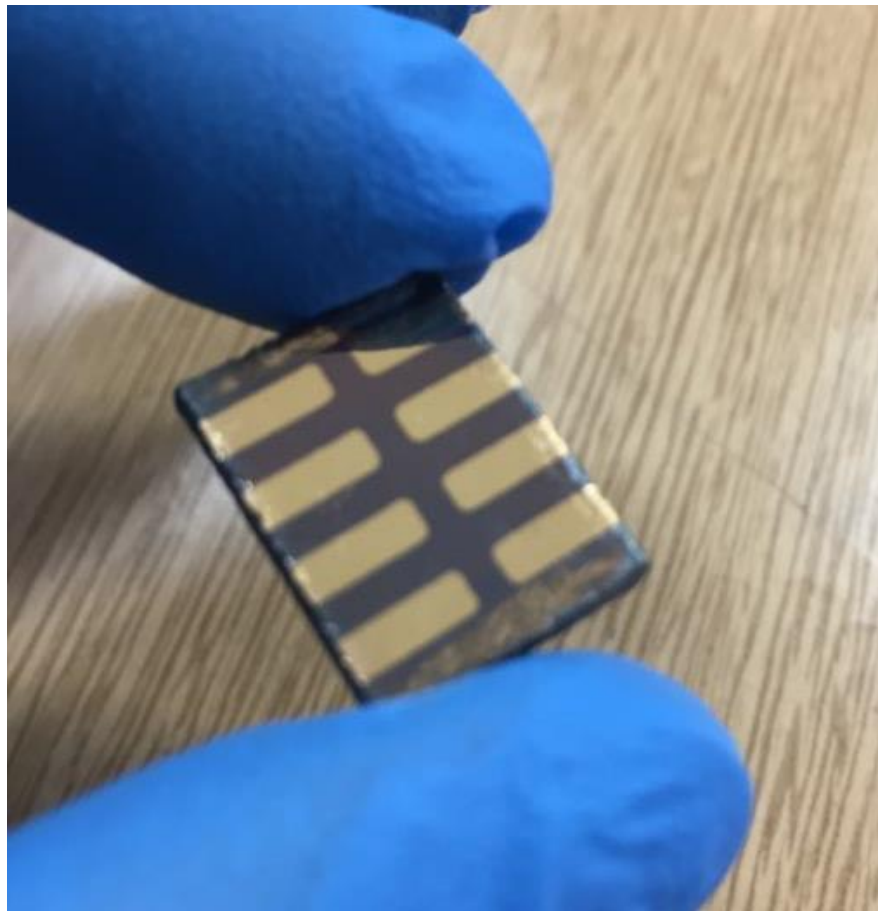
Figure 3.3. Image of fabricated perovskite devices in this study.

CHAPTER 4

RESULTS AND DISCUSSION

In this work, studies have been conducted to construct perovskite solar cells employing copper thiocyanade (CuSCN) layer as a hole transport layer and characterizations were made in order to examine structural and electronic properties of these films and their effect on the performance of the cells. X-ray diffraction patterns of CuSCN film were registered by Rigaku D/MAX 2200/PC with Cu Kα radiation. Devices were investigated morphologically using scanning electron microscopy (FEI Quanta 400 FEG equipped with EDX analyzer). CuSCN films were characterized by X-ray photoelectron spectroscopy (XPS) and ultraviolet photoelectron spectroscopy (UPS) (PHI 5000 VersaProbe) for analysis of chemical and electronic properties. Morphological features of the films were also determined by atomic force microscopy (AFM) (Veeco CP II). Optical properties of the films were examined by UV-Vis measurements (Ocean Optics USB-ISS) and visible light transmission of the films were recorded between 300-900 nm wavelength. To investigate total performances of the cells, Yokogawa GS610 source measure unit under simulated AM 1.5 conditions were used to record J-V curves of prepared solar devices with Newport solar simulator 67005. Moreover, electrochemical impedance spectroscopy was conducted using Gamry reference 3000 under illumination with white LED light (60 mW/cm^2) and fitting was conducted by Echem analyst software with the equivalent circuit.

4.1   X-Ray Analysis of CuSCN Thick Film

XRD analysis of CuSCN layer were performed from thick layer on glass substrate which is used as hole transport layer in produced perovskite solar cells. X-Ray spectra of the layer were recorded for angles between 10-80° for CuSCN. The XRD

pattern of the prepared CuSCN thick layer on the glass substrate is shown in Figure 4.1. Observed diffraction peaks could be well matched to the rhombohedral crystal orientations, which is coherent with JCPDS card No. 29-0581. The prominent peaks monitored at 2θ angles of 16.16º, 27.22º, 32.64º, 34.58º, 47.07º, 49.82º, 55.26º, 58.48º, 59.73º, 62.30º, 68.94º, and 75.44º are appointed scattering from the (003), (101), (006), (104), (110), (009), (021), (116), (024), (205), (027), and (211) planes of the CuSCN crystal without impurity peaks. Sharpness of the diffraction peaks in the pattern indicate the good crystallinity of the deposited CuSCN layer.
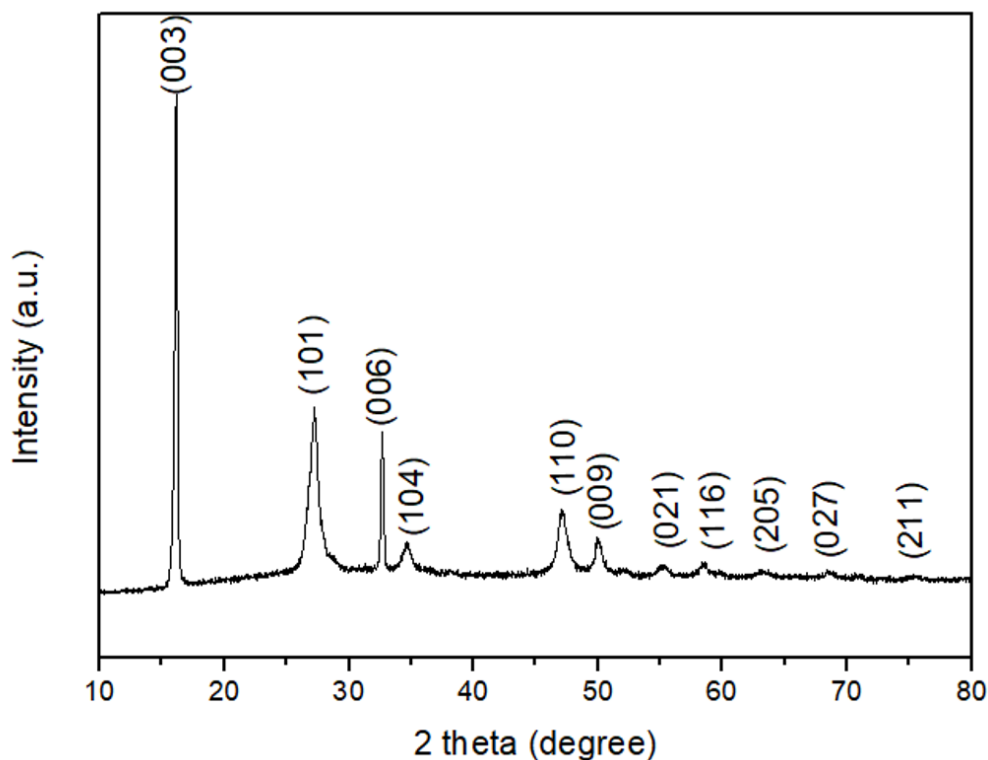
Figure 4.1. XRD pattern of CuSCN thick film deposited on glass substrate.

4.2 Topographic Analysis of CuSCN Thin Films

The topography of CuSCN thin films on perovskite layer are analysed using atomic force microscopy (AFM) (Figure.4.2) and scanning electron microscopy (SEM) (Figure.4.3). 4.5 μm x 4.5 μm 2-D observation on the AFM scans were used to

estimate the maximum height and roughness of the spin coated thin CuSCN layer. The dark brown to white contrast displayed alongside the AFM scan image in Figure 4.2 represents the height scale of the AFM scans. The surface roughness value which is determined by 2-D AFM scan was determind as 19.46 nm and the observed average height in surface scan was 75.58 nm.
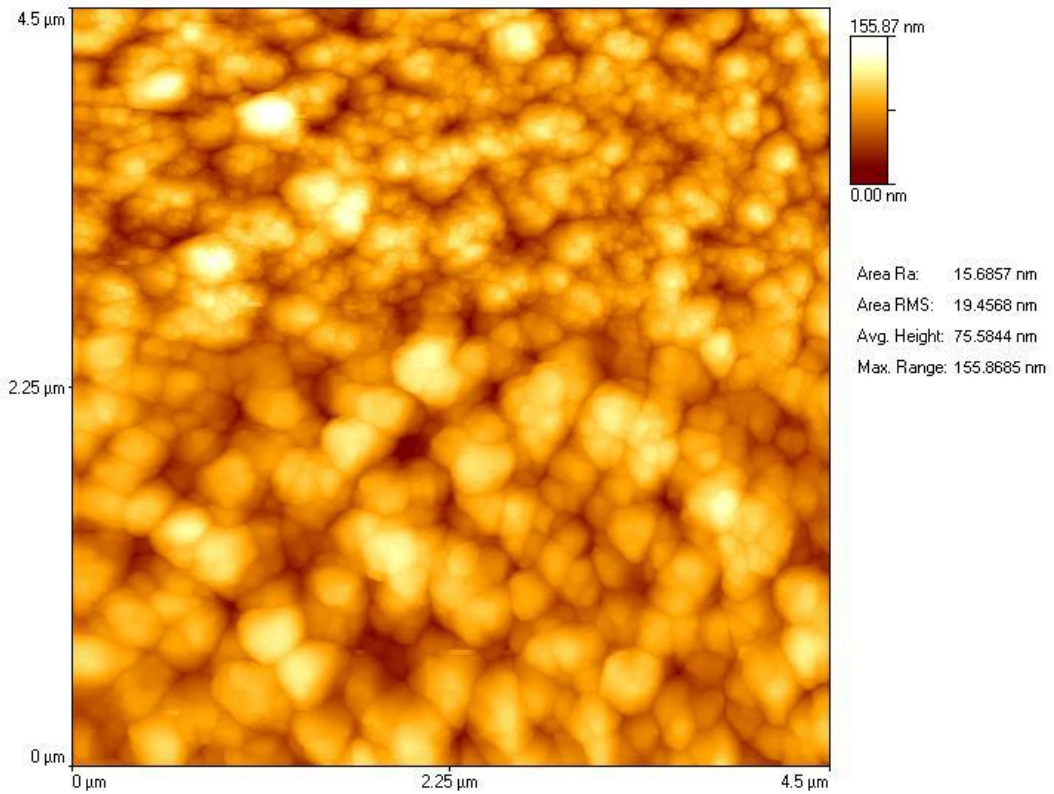
Figure 4.2. 4.5 µm x 4.5 µm 2-D AFM scan on the surface of CuSCN layer.

Two dimensional AFM surface scans and SEM images support the allocation of the CuSCN layer and both confirm the homogeneity of the fabricated layers. The measured values are in a good agreement with SEM approximation.

| WD | mag | HV | HFW | ⸺ 1 µm ⸺ |
| 6.2 mm | 100 000 x | 20.0 kV | 2.98 µm | METE-METU |
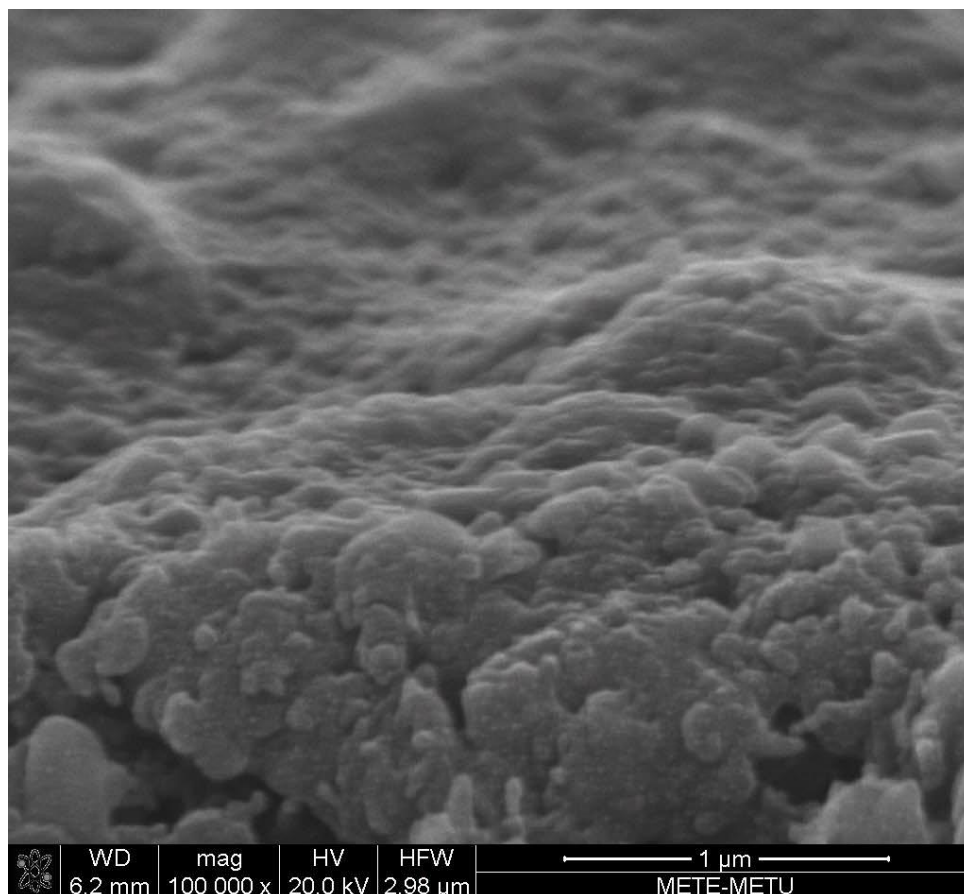
Figure 4.3. SEM image of CuSCN layer on perovskite.

4.3   X-ray Photoelectron Spectroscopy (XPS) Analysis of CuSCN Layer

In order to get accurate quantitative and qualitative information about the chemical compositions and state of the elements in the prepared CuSCN film on glass substrates, high resolution XPS spectra of the characteristic regions were recorded and submitted for the CuSCN film. The XPS survey spectra in this study specify the presence of the expected elements which are copper (Cu), sulfur (S), carbon (C), and nitrogen (N).

In Figure 4.4 high resolution XPS specta of Cu is shown. The main peak of the copper Cu $2p^{3/2}$ spectrum at 931.6 eV which is shown in Figure 4.4 corresponds to

Cu (I). There is no peak observed from some contributions such as Cu (II) which can be positioned at higher energies.

The spectrum in the sulfur 2p region has been fitted by a series of 3 doublets of S $2p^{3/2}$ and S $2p^{1/2}$ each. Once again, the spectrum is dominated by a large signal with $2p^{3/2}$ peak situated at 162.0 eV, which was ascribed to a sulfur atom in –S-C form as shown in Figure 4.5.
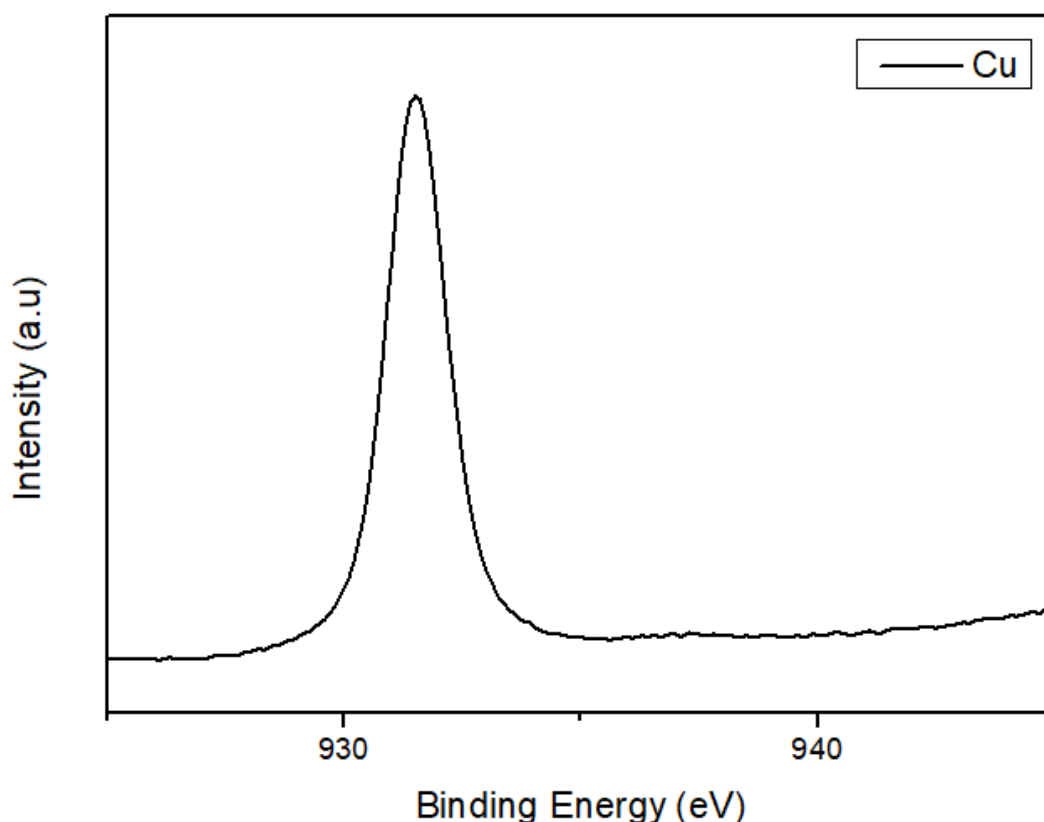
Figure 4.4. High resolution XPS spectra of Cu taken from CuSCN layer.

Observed XPS spectra of C includes C 1s aliphatic and C 1s, -SCN. The peak at 284.6 eV, which was also used for the calibration of the whole spectrum, is ascribed to the aliphatic carbon sp^3 impurities present on the surface, while the peak at the highest energy (286.5 eV) corresponds probably also to the adventitious -SCN form (Figure 4.6) [181].
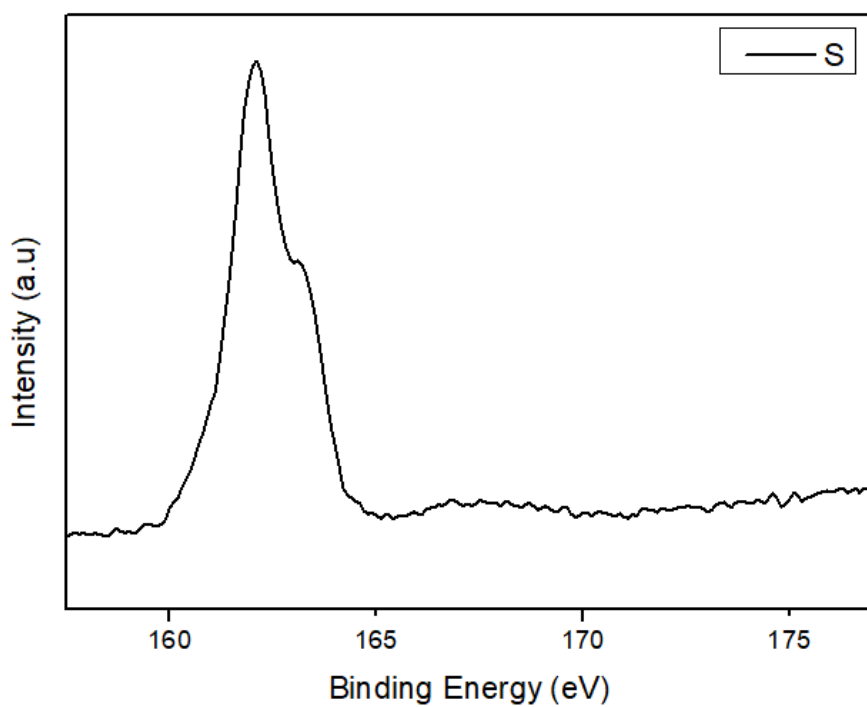
Figure 4.5. High resolution XPS spectra of S taken from CuSCN layer.
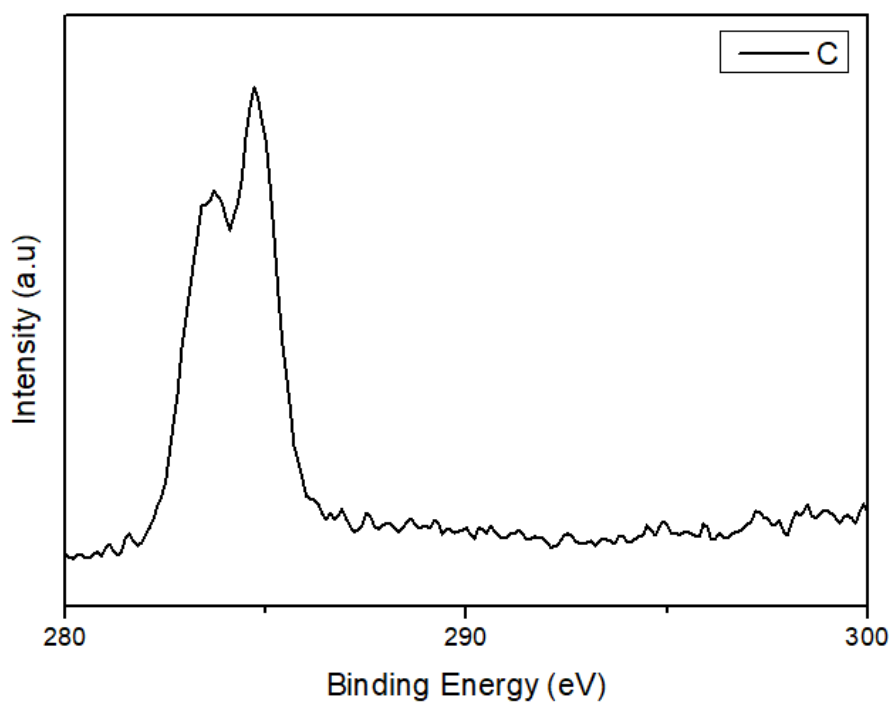
Figure 4.6. High resolution XPS spectra of C taken from CuSCN layer.

The XPS spectrum of N is shown in Figure 4.7. Observed major peak at 397.3 eV from 1s region and probably corresponds to the nitrogen in a nitrile form (N≡C) as described in the literature [181].
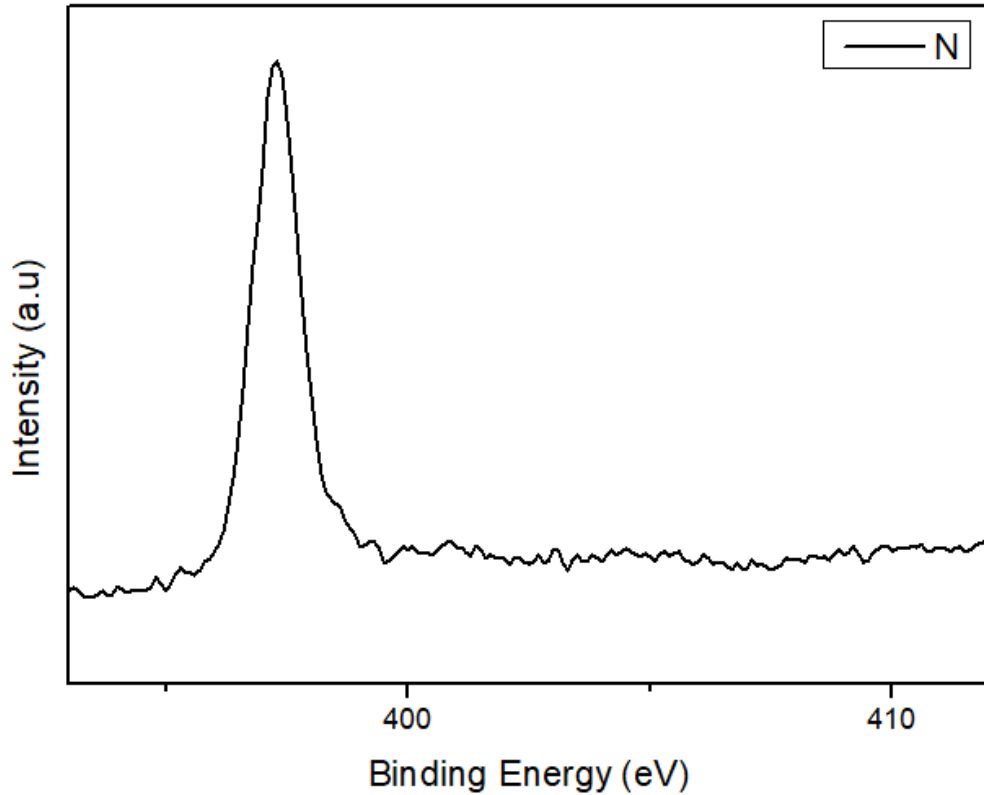
Figure 4.7. High resolution XPS spectra of N taken from CuSCN layer.

4.4   Electronic Characterization of CuSCN Layer

Ultraviolet photoelectron spectroscopy (UPS) was studied to indicate electronic structure of the CuSCN layer produced with spin coating technique by HeI emission (21.21 eV) and observed spectrum was given in Figure 4.8. The cut-off energy (16.07 eV) which was extracted from UPS spectra concerned with work function of CuSCN layer where the fermi level is located to 5.14 eV with respect to vacuum level [182].
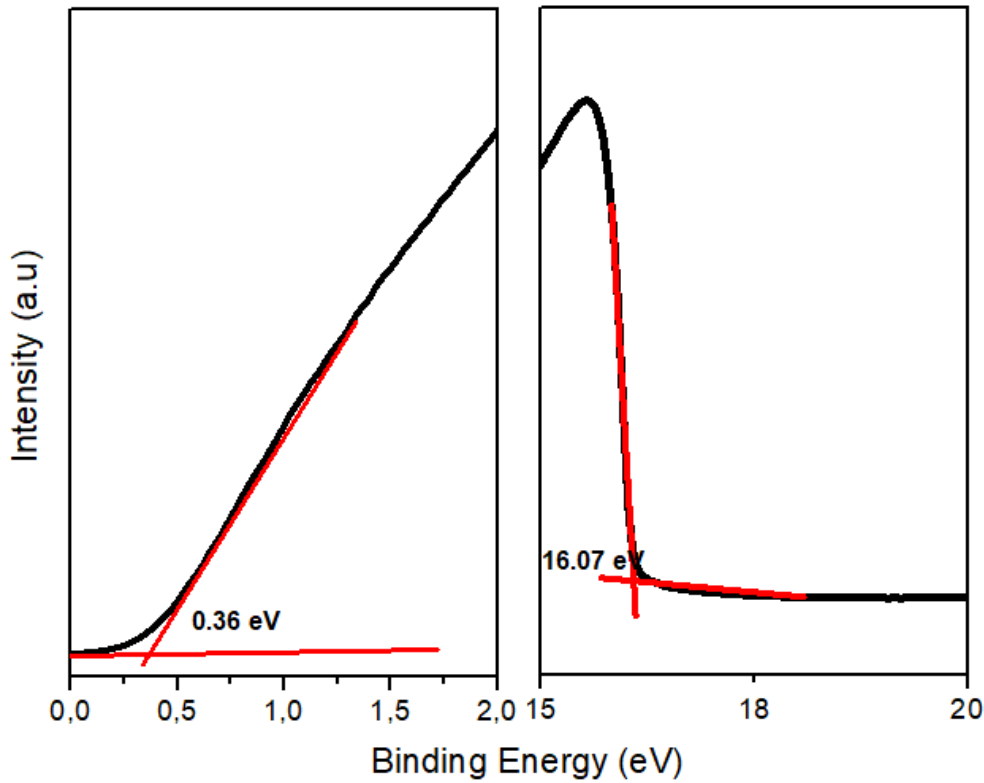
Figure 4.8. UPS spectra of the CuSCN layer placed in the perovskite cells at the onset and cut-off energies.

The onset energy in UPS spectra gives difference between valence band maximum (VBM) and the fermi level of CuSCN layer and it was calculated to be 0.36 eV (Figure 4.8). Therefore, VBM is located to 5.50 eV when multiplying calculated Fermi level with onset energy. Location of the conduction band minimum is calculated to be 1.64 eV by adding the optical band gap value of 3.86 eV which is extracted from the Tauc plot given in Figure 4.9 by the light transmission spectra of the spin coated CuSCN layer on quartz substrates. The fermi level located at 0.36 eV above the valence band maximum is also positioned below the center of the band gap and it advocates the p-type character of the CuSCN film. The calculated band diagram of the CuSCN layer in this work is described in Figure 4.10 with respect to perovskite layer.
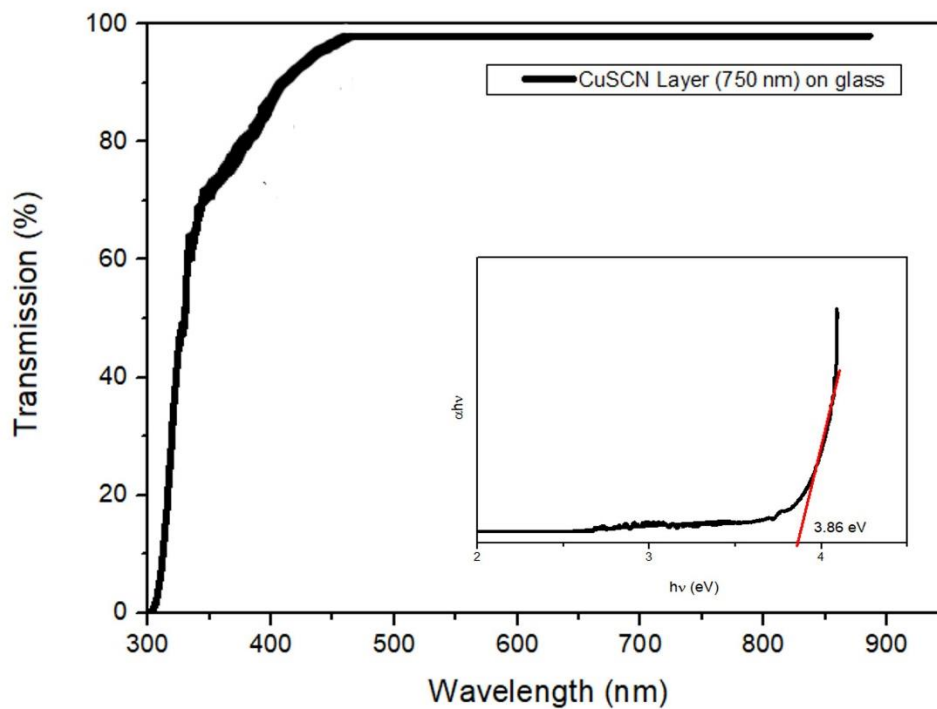
Figure 4.9. UV-Visible light transmission spectra of the layer deposited on glass substrates and Tauc plot showed in the inlet image.

It is seen that the difference between perovskite layer and VBM of the CuSCN layer was found to be 0.07 eV and close to each other which can be negligible. The large difference between conduction band minima (CBMs) of CuSCN and perovskite layer insures prevention of electron transfer from perovskite to CuSCN and demonstrates CuSCN as an effective electron blocking layer in the cells.
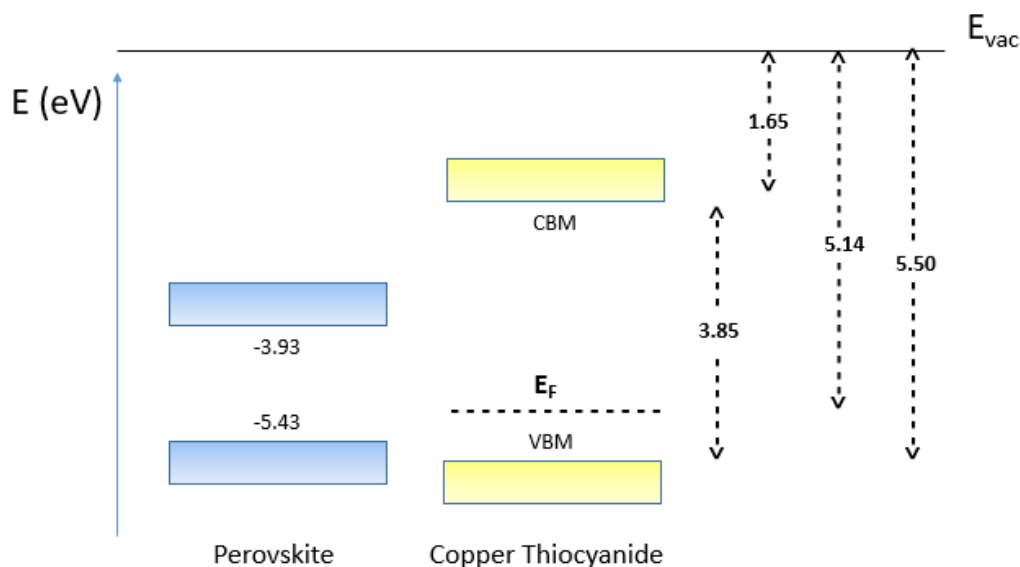
Figure 4.10. Band diagram of copper thiocyanide films showing the conduction band minimum (CBM), valence band maximum (VBM), and fermi level (E$_f$) acquired from UPS measurements with respect to that of perovskite.

4.5   Characterizations of Cells

Copper thiocyanide material employed as a hole transport layer of perovskite solar cells are characterized by a solar Simulator using AM1.5 simulated light and J-V curves were obtained to compare layer thickness on the performance of the devices. Stock solution of CuSCN in diethylsulfide were used to spin coat deposition of CuSCN layers on perovskite layer to behave as a hole transport layer. Architecture of fabricated cells also comprises of a dense and a mesoporous TiO$_2$ layers for electron transportation, a perovskite layer introduced inside the mesoporous TiO$_2$ layer and as a separate capping layer. Then, CuSCN films were deposited on top of perovskite layer forming a mesoporous n-i-p architecture solar cell (Figure 4.11).
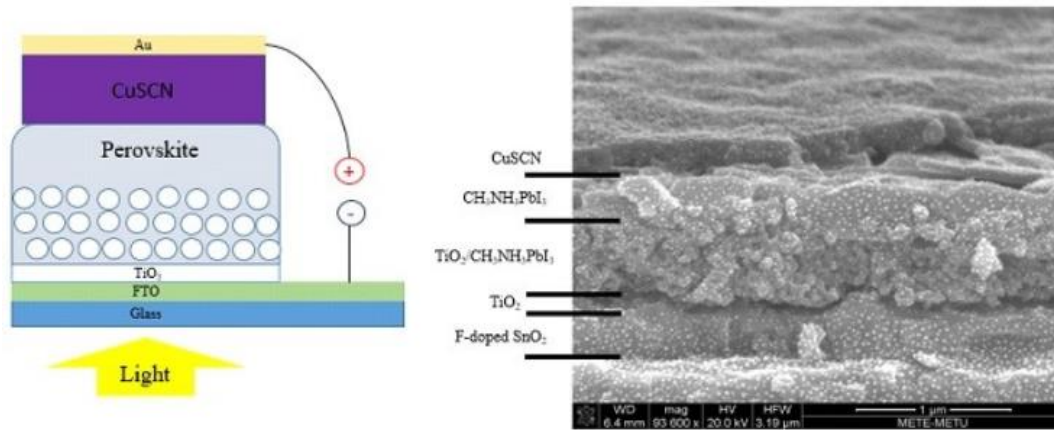
Figure 4.11. **(a)** Schematic illustration of mesoscopic n-i-p configuration of perovskite solar cell constructed in this work. **(b)** Cross sectional SEM image of the cells.

For the state of n-i-p structure, confected stock solution of CuSCN should be spinned straight forwardly on the perovskite layer, so a constraint for solution media emerges because many solvents used to dissolve CuSCN also dissolve the perovskite crystals and degrade the perovskite layer. In addition, other solvents used for CuSCN precursor preparation need high temperature treatment for removal of them. Therefore, they can not also be employed because of the degradation of perovskite layer at the heat treatment temperatures above 150ºC. When these non-removed residual molecules of solvents remain in the cell, they prevent charge transfer between the layers. From cross sectional SEM image given in Figure 4.11, particular layers can be seen and there is no evidence of physical damage associated with degradation of perovskite layer due to diethylsulfide solution medium used for CuSCN deposition. Accomplished cells after Au contact metal evaporation were characterized under AM1.5 conditions and J-V curves of cells with different CuSCN layer thicknesses are shown in Figure 4.12 and performance parameters are tabulated in Table 4.1.

Power conversion efficiency (η) of a solar cells is elementally the ratio of maximum power output P_{MP} of the solar cell to the power of incoming light P_{in} given by [183]:

$$\eta = \frac{P_{MP}}{P_{in}}$$

<div align="right">Eq. [4.1]</div>

The highest product value of potential and current gives the maximum power point, which is described as maximum power output of the solar cells when a load is connected to the device. There is no current flowing inside the cell in open circuit conditions, therefore voltage has the maximum value. Current has maximum value in short circuit conditions, when there is no potential difference. Open circuit voltage and short circuit current values of the cell begin to decrease in actual conditions with a load on the circuit. Therefore, product of potential and the corresponding current value at their maximum defines the maximum power output of the cell. This maximum product value of the current and potential depends on the ability of solar cells to provide as much power as feasible to the load on the cell which is named by the fill factor (FF) of the cell. Fill factor is mostly affected by electron losses inside the cell and the internal resistances of the cells which is a helpful quantity for characterizations of solar cells. Fill factor value is identified by the ratio of maximum current I_{MP} and voltage V_{MP} product to the short circuit current I_{SC} and open circuit voltage V_{oc} product as [183]:

$$FF = \frac{I_{MP} V_{MP}}{I_{OC} V_{OC}}$$

<div align="right">Eq. [4.2]</div>

Production conditions and sizes of the cells influence the performance and fill factor of the cells, so it is important to fabricate cells with identical active areas and to avoid additional resistive elements.

Cells yielded 3.18% power conversion efficiency when prepared without a hole conductor layer due to natural p-type behaviour of perovskite layer itself which can possess a depletion layer together with an n-type mesoporous scaffolding layer and have hole conducting skill as exemplified by former studies [184,185]. Employment of CuSCN layer in the cell increases both short circuit current and open circuit

voltage concurrently. In addition, excessive enhancement was achieved while CuSCN is used as a hole transporting layer. By optimizing CuSCN layer thickness with the concentration of CuSCN particles in diethylsulfide, champion cell was succeeded having 11.02% of power conversiyon efficiency. The enhancements in V_{oc} and J_{sc} values of devices are simultaneously related to surface coverage of CuSCN layer and homogeneous coating. For all observed J-V curves of constructed cells, no S-shaped J-V characteristic was encountered. This can be explained such that CuSCN layer does not cause resistance for hole transportation which is mostly associated with the problem of interfacial excessive resistance or charge conduction [186].
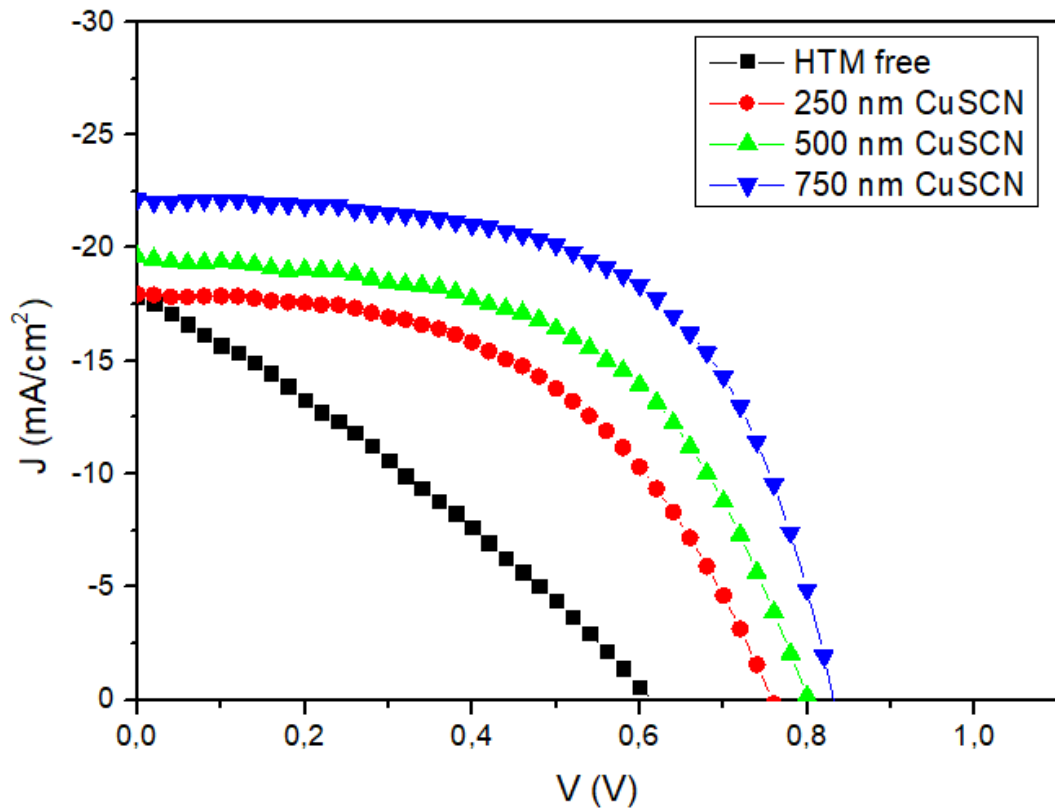
Figure 4.12. J-V curves of the hole conductor free and CuSCN based cells with different concentrations under simulated AM 1.5 conditions.

750 nm thick CuSCN layer as a hole conductor yielded the best performances reached in this study with an open circuit voltage value of 0.83 V which outperforms cell without hole conductor. Fill factor was also rised up to 0.60 yielding an overall efficiency of 11.02% for the best cell measured at 500 mV/s under forward scan (from Jsc to Voc) conditions. Further decrease in the concentration of CuSCN for the same spin rates causes non homogeneous distribution of the CuSCN particles and it does not allow the deposition of continuous CuSCN films. The engagement of FF value on the concentration and efficiency of the cells can be explained by partial agglomeration of the film which was highly dependent on the concentration of CuSCN particles.

Table 4.1. Acquired performances of the cells produced using different HTM layer thicknesses.

Cell Configuration	Efficiency (%)	V_{oc} (V)	J_{sc} (mA)	FF
50 nm BL + 250 nm mesoporous TiO_2 + HTM free	3.18	0.61	17.82	0.29
50 nm BL + 250 nm mesoporous TiO_2 + 250 nm CuSCN	6.89	0.75	17.96	0.51
50 nm BL + 250 nm mesoporous TiO_2 + 500 nm CuSCN	8.44	0.81	19.61	0.53
50 nm BL + 250 nm mesoporous TiO_2 + 750 nm CuSCN	11.02	0.83	22.15	0.60

Recombination resistances and charge transport resistances are the most critical parameters in device performance of perovskite solar devices so it is essential to explain them. In order to determine the contribution of CuSCN layer on cell performance in depth, both without hole transporter and CuSCN included as hole transporter cells were qualified with impedance spectroscopy (IS) analysis. IS is a strong method to explain recombination kinetics and charge transportation phenomena in solar devices and have been used for characterization of perovskite solar cells. In this study, IS spectra of the devices were registered under white LED with constant illumination of 60 mW/cm^2 applied in varied bias voltages. There are two distinct arcs detected in Nyquist plots for both types of cells (HTM free and CuSCN as HTM layer) at 0 mV and 500 mV applied bias voltages which are given in Figure 4.13-a and b. There are no Gerischer feature or transmission line detected in mesoporous solar devices, because of 250 nm thickness of TiO$_2$ mesoporous layer held constant throughout this work [187]. The impedance spectra were fitted using a simple equivalent circuit model given in the inlet image of Figure 4.13-a. Charge transfer resistances (R_{CT}) associated with the first observed arc emerging in high frequency region are related to capacitances in the charge selective contacts which are CuSCN hole transporting layer, TiO$_2$ dense blocking and mesoporous layers [188,189]. In order to reach better fitting of observed spectrum, capacitances are represented with a constant phase element (CPE_{CT}) rather than ideal in equivalent circuit because both selective contacts contain pin holes and might not fully cover the cell. Otherwise, the low frequency arc in impedance spectroscopy is associated with recombination capacitance (CPE_{REC}) and resistance (R_{REC}).
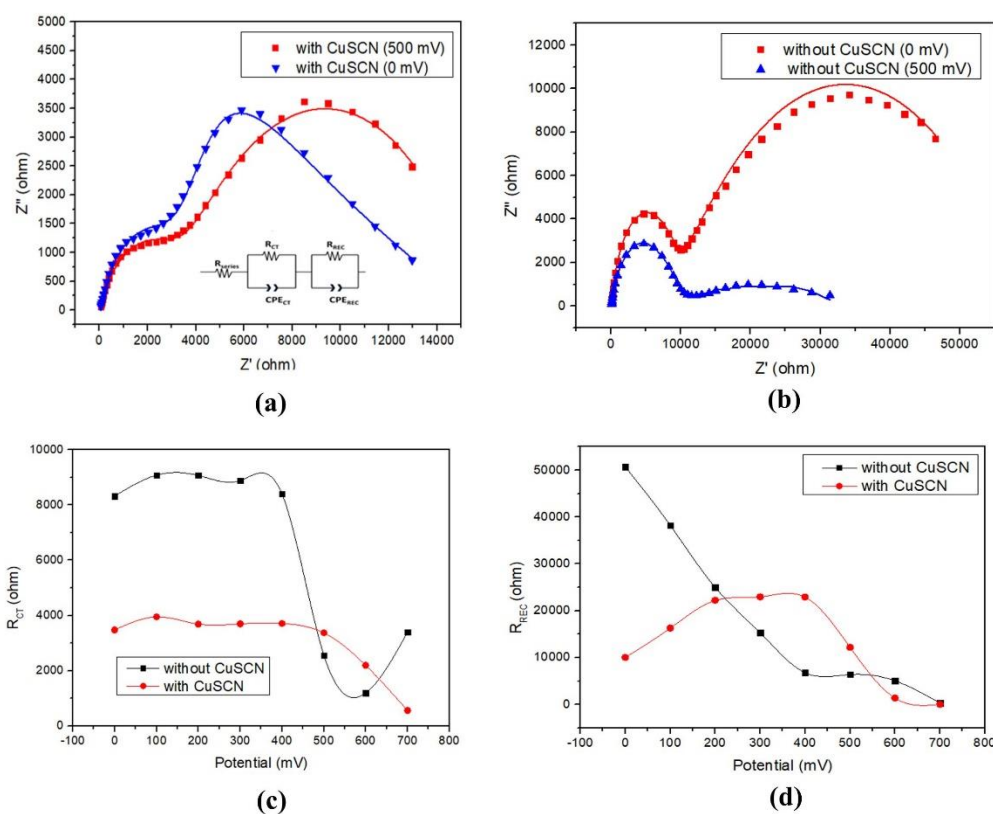
Figure 4.13. **(a)** Nyquist plots of the CuSCN layer included perovskite solar cell structure under 0V and 0.5V applied bias. Equivalent circuit model used to fit impedance data is also shown in the inlet image. **(b)** Nyquist plots of hole conductor free devices under 0V and 0.5V applied bias. **(c)** Charge transport resistances of two different configuration cells with increasing applied voltage. **(d)** Recombination resistances of two different configuration cells with increasing applied voltage.

Charge transfer resistances of the studied cells at applied bias voltages are shown in Figure 4.13-c. As long as mesoporous and blocking TiO_2 layers are the same for both cell types, charge transfer resistances are explained by hole transfer medium.

Addition of CuSCN layer as a hole transport material introduces a net decrease to the charge transfer resistance of the cells, almost two times higher than hole conductor free cell. Hopping mechanism is the dominant carrier transport pathway which is main factor for electrical resistance for inorganic p-type included devices

48

contrary to polymeric dense hole conductors. However, authentic contribution of the CuSCN layer evinces itself as an increased recombination resistance given in Figure 4.13-d. Recombination resistanceof CuSCN included cells is higher than the hole conductor free devices at 300 to 500 mV applied potential. At 0 V, hole conductor free cell shows a higher resistance to recombination competing with CuSCN based cell because of no current collecting at low applied voltages. However, when voltage increases, a sharp drop was observed in the recombination resistance in hole conductor free cell. Meanwhile, studied cells with CuSCN layer can endure recombination up to 0.4 V applied bias voltage. This skill of resistance to recombination makes CuSCN a perfect inorganic hole blocking material and this ability mostly derives from low electron affinity of CuSCN. Increased resistance to recombination in CuSCN included cells is the main advantage and leads to the efiicient power conversion by enhancement in V_{oc}, J_{sc}, FF, and stability contrasted to hole conductor free cells.
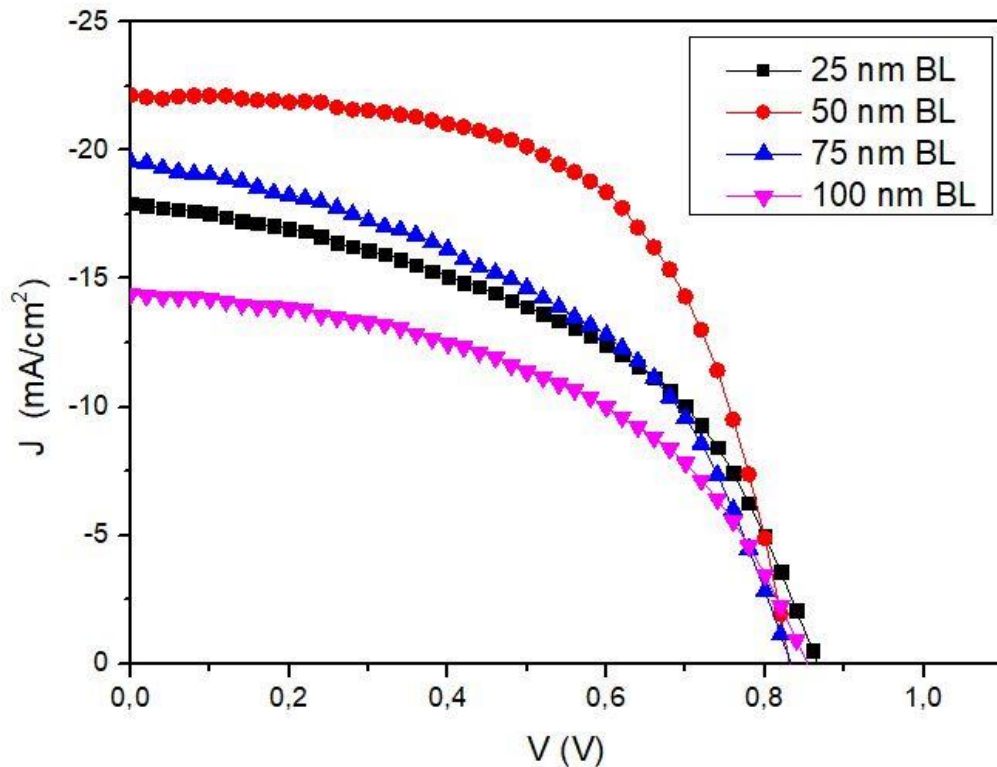
Figure 4.14. J-V curves of the CuSCN based cells with different different blocking layer thicknesses under simulated AM 1.5 conditions.

The thicknesses of other layers such as mesoporous (mp) and compact blocking TiO$_2$ layers are also studied with the same configuration. Compact TiO$_2$ layer that is produced by sputtering in different thicknesses acts as hole blocking layer in the cell. J-V curves of different blocking layer included cells are given in Figure 4.14 and cell performances are also tabulated in Table 4.2. The best cell performance was obtained by deposition of 50 nm BL due to its highest Jsc value where Voc values of cells with different BL thicknesses remain almost same.

Table 4.2. Acquired performances of different blocking layer thicknesses used in the construction of cells.

Cell Configuration	Efficiency (%)	V_{oc} (V)	J_{sc} (mA)	FF
25 nm BL + 250 nm mesoporous TiO$_2$ + CuSCN	7.47	0.87	17.95	0.47
50 nm BL + 250 nm mesoporous TiO$_2$ + CuSCN	11.02	0.83	22.15	0.60
75 nm BL + 250 nm mesoporous TiO$_2$ + CuSCN	7.68	0.83	19.56	0.47
100 nm BL + 250 nm mesoporous TiO$_2$ + CuSCN	6.02	0.85	14.41	0.49

Differences in charge transfer resistances which are calculated from IS study at 0.4 V and showed in Figure 4.15 are also consistent with cell performances. The lowest charge transfer resistance was reached by construction of cell with 50 nm BL which increases J_{sc} value. 50 nm is the optimized thickness of this layer, and more or less than this value of thickness gives undesirable effects in the cell as explained by IS study.
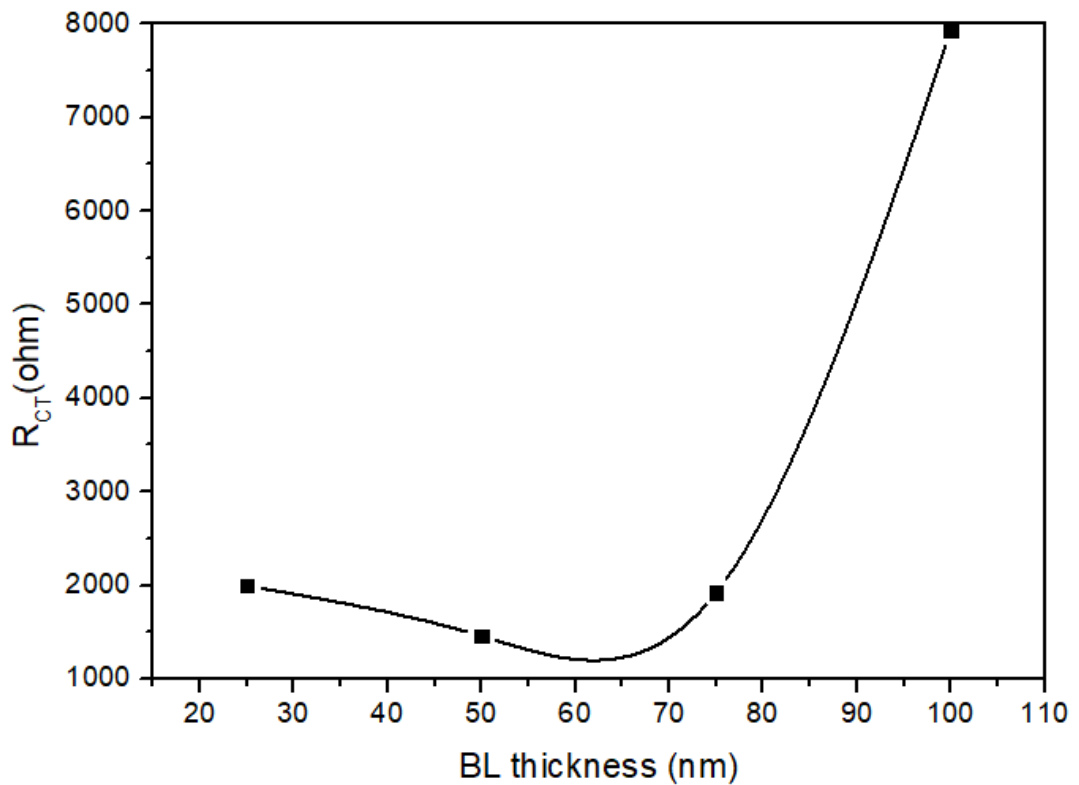
Figure 4.15. Charge transport resistances of cells with different blocking layer thicknesses at 0.4 V.

mp-TiO$_2$ layers with different thicknesses were investigated using SEM and obtained images are given in Figures 4.16, 4.17 and 4.18. mp-TiO$_2$ layer not only affects charge transfer resistance but also influnces recombination resistance of the cells. Due to lowest charge transfer resistance with highest recombination resistance that was calculated from IS study, 250 nm of mesoporous layer was optimized and gives best performance with an enhancement in Voc and Jsc values.
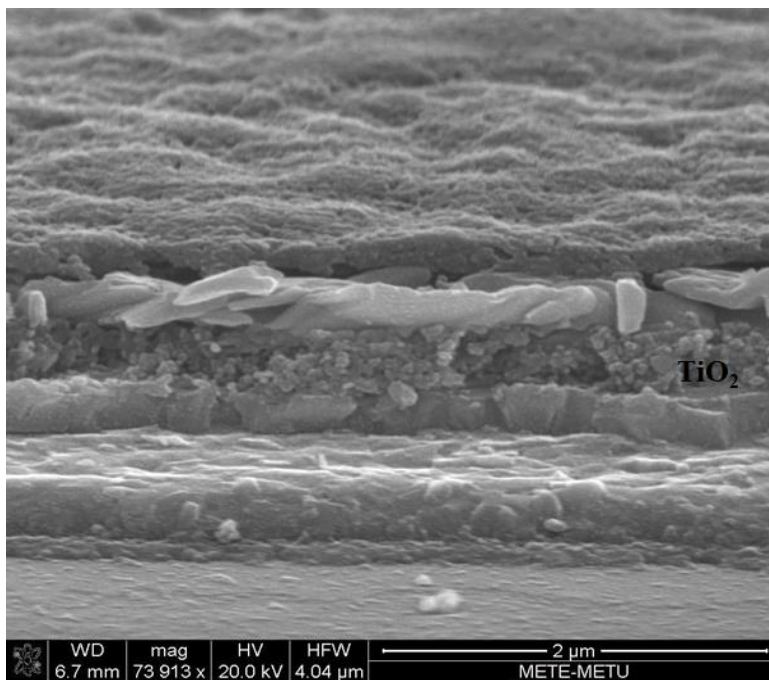
Figure 4.16. Cross-section SEM images of cells constructed using 250 nm mp-TiO$_2$ layer.
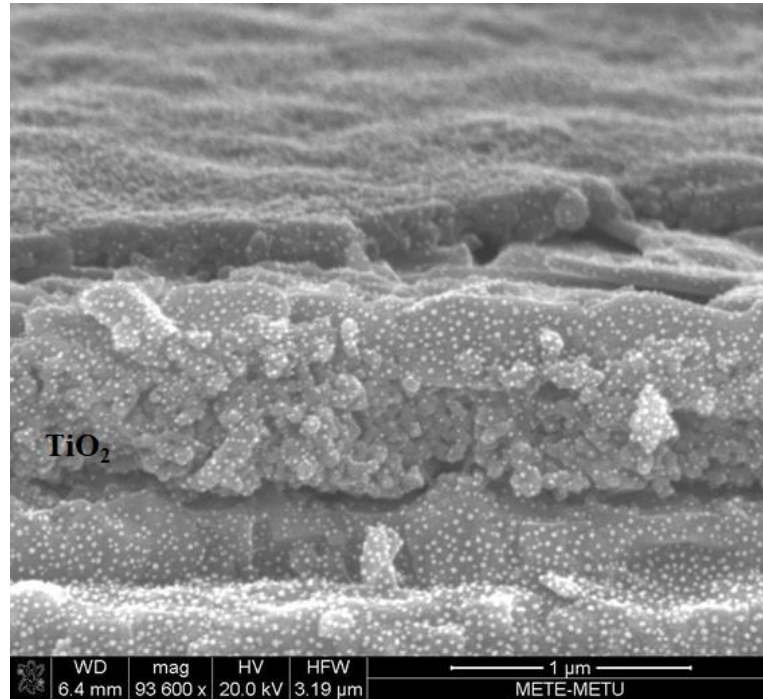
Figure 4.17. Cross-section SEM images of cells constructed using 500 nm mp-TiO$_2$ layer.
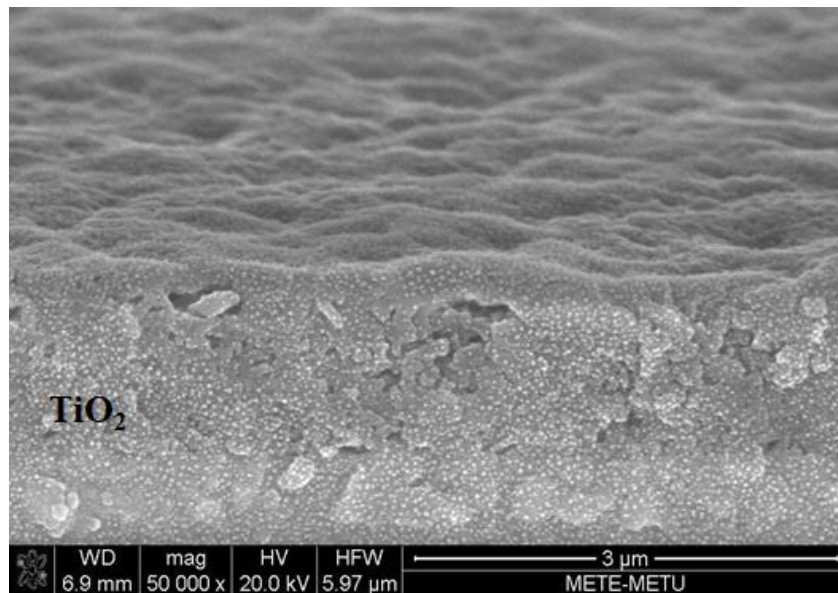
Figure 4.18. Cross-section SEM images of cells constructed using 750 nm mp-TiO$_2$ layer

Table 4.3. Acquired performances of different mesoporous TiO$_2$ thicknesses used in the construction of the cells.

Cell Configuration	Efficiency (%)	V$_{oc}$ (V)	J$_{sc}$ (mA)	FF
50 nm BL + mesoporous TiO$_2$ free + CuSCN	5.65	0.71	17.84	0.44
50 nm BL + 250 nm mesoporous TiO$_2$ + CuSCN	11.02	0.83	22.15	0.60
50 nm BL + 500 nm mesoporous TiO$_2$ + CuSCN	7.52	0.89	18.82	0.45
50 nm BL + 750 nm mesoporous TiO$_2$ + CuSCN	4.25	0.75	15.00	0.38
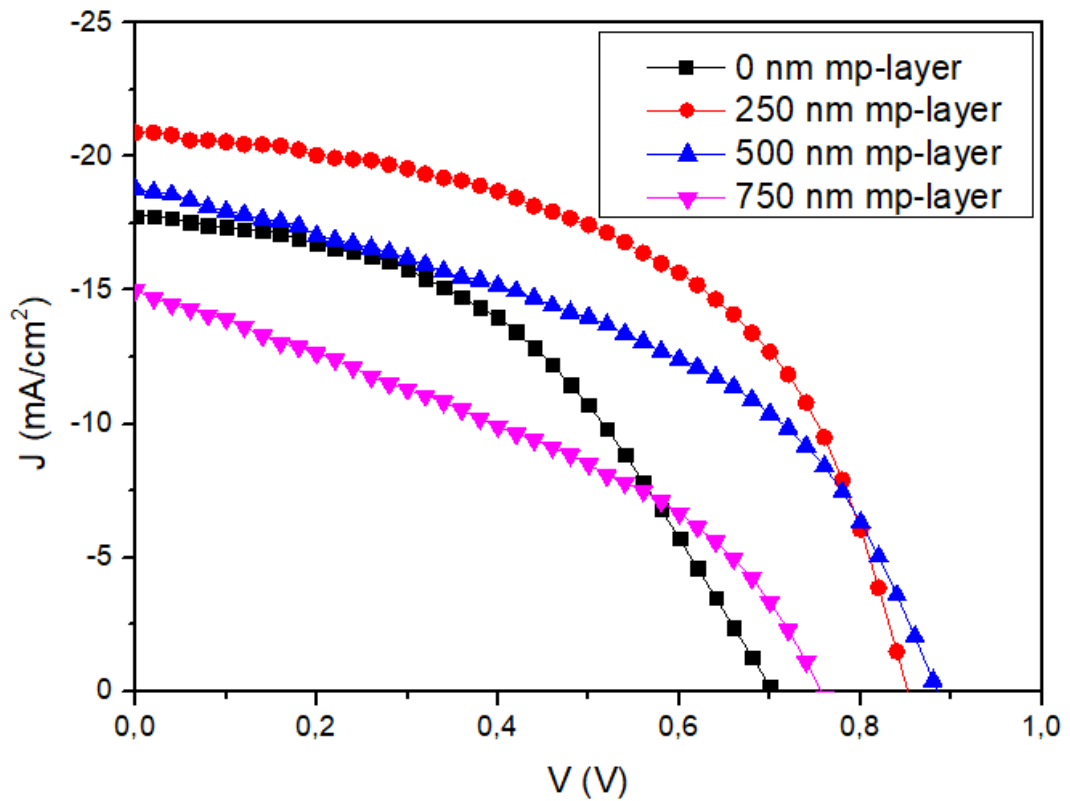
Figure 4.19. J-V curves of the CuSCN based cells with different mp-layer thicknesses under simulated AM 1.5 conditions.

Enhancement in J_{sc} shows a decrease in charge transfer resistance and an increase in V_{oc} is related to enhancement in recombination resistance of the cells. J-V curves which were given in Figure 4.19 and tabulated cell performances in Table 4.3 are consistent with IS study. mp-layer free cell was not resistant to recombination generations and this is the main reason of decrease in V_{oc}. Although V_{oc} values were nearly identical with 250 and 500 nm mp-layer included cells, enhancement in J_{sc} value was acquired using 250 nm mp-layer due to lower charge transfer resistance. The high efficiency of the cell produced using 250 nm thick mp-layer depends on not only low charge transfer resistance but also on high recombination resistance which is shown in Figure 4.20.
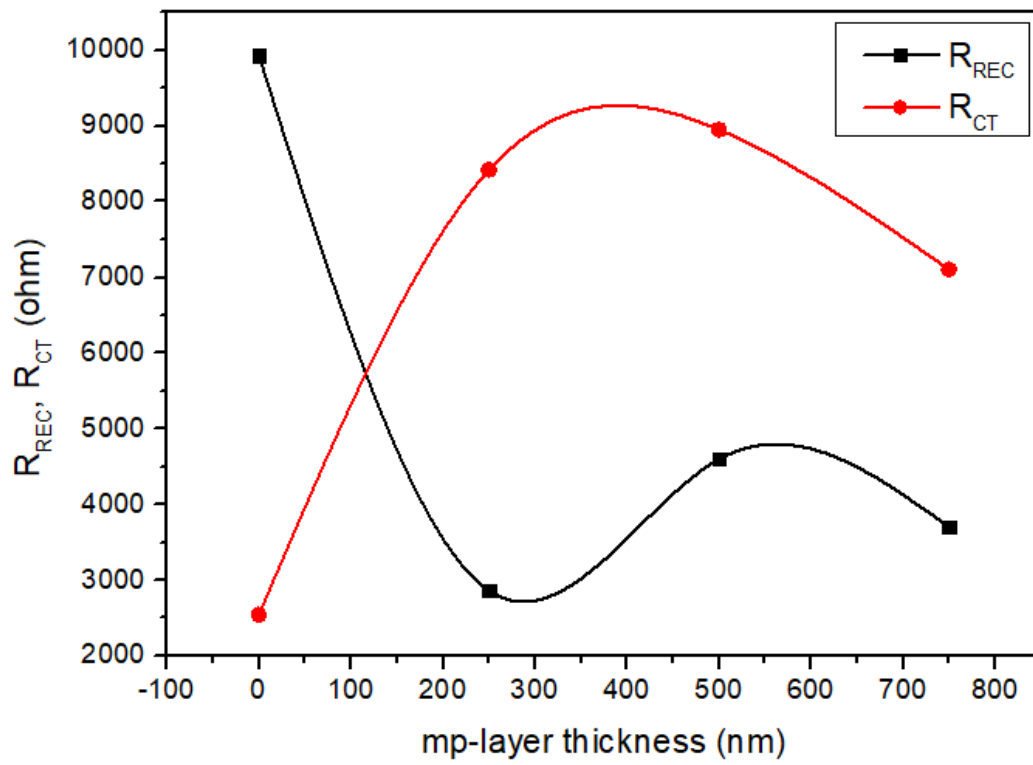
Figure 4.20. Charge transport resistances and recombination resistances of cells with different mesoporous layer thicknesses at 0.4 V applied voltage.

CHAPTER 5

SUMMARY AND CONCLUSIONS

In this work, perovskite solar cells were succesfully produced employing copper (I) thiocyanate as a hole conducting material which was characterized by XRD, XPS, AFM, UV-Vis, UPS, SEM and J-V measurements. This work also includes effects of all extraction layers in the performance of the cell which were optimized by J-V characterizations.

As the hole transporting material in perovskite solar cells, diethylsulfide was used to solve CuSCN powder and solution deposition method was employed to produce CuSCN layer without degrading the perovskite layer. There are many methods for CuSCN deposition on perovskite layer in the literature. However, most of solution based deposition methods of CuSCN requires solvents which have the polar character. Because of this restriction, studies of CuSCN material as hole transporting layer in the literature are mostly in p-i-n inverted structures using electroplating techniques for CuSCN layer deposition.

Peaks found in XRD and XPS studies of deposited thick CuSCN layers using solution based spin coating technique are in good agreement with the data in the literature. XRD results also show the good crystallinity of deposited layer. The XPS survey spectra in this study specify the presence of the expected elements which are copper (Cu), sulfur (S), carbon (C), and nitrogen (N).

Electronic characterizations of CuSCN layer were performed by UV-Vis and UPS measurements. Tauc plot analysis were performed to determine band gap of CuSCN layer using UV-Vis light transmission spectrum. Although, the difference between cut off energy extracted from UPS specta and HeI emission gives the Fermi level

position of CuSCN layer, the onset energy is required to determine VBM of the film. CBM position of the CuSCN film was calculated by adding the band gap value found from Tauc plot. Thus, the results show that CuSCN layer has p-type character and is convenient for hole transporting layer in perovskite solar cell due to suitable band positions with respect to perovskite material.

Fabricated n-i-p configurated mesoporous perovskite solar cells using CuSCN hole transporting layer and CuSCN free were characterized by recording J-V curves under illumination. Efficiencies and fill factors of the cells are calculated from J-V curves. CuSCN included cells were obtained drastically efficient compared to hole conductor free cells. The champion cell obtained in this study with thick and dense CuSCN layer reached 11.02% efficiency and 0.60 fill factor value. The effects of mesoporous and dense blocking TiO_2 layer thicknesses in cell performances were also studied and results were evaluated by charge transfer kinetics. Although there was no change in potential of cells with the thickness of blocking layer, which is dense and compact TiO_2, the current flow in the cell was different due to electron transportation. However, the thickness of mesoporous TiO_2 layer affects not only the current but also potential of the cells. Because, mesoporous layer has to prevent recombinations with efficient charge transfer in perovskites. Results derived from J-V measurements were also consistent with IS analysis. IS analysis were also used to clarify recombination and charge transfer resistances of the cells.

In conclusion, diethylsulfide was used to solve CuSCN powder and solution deposition method was employed to produce CuSCN layer without degrading the perovskite layer. Solution deposition of CuSCN on perovskite layer in mesoporous n-i-p configuration enhanced the efficiency of the cells compared to the HTM free cells. The presence of CuSCN as a HTM leads to an enhancement to 11.02 % overall efficiency through increases in V_{oc} and J_{sc}. This simple deposition method of CuSCN layer on perovskite allows to establish n-i-p configurated perovskite solar cells with CuSCN or other inorganic metal oxide materials as a hole transporting layer, thus replacing expensive and long term instable polymeric structures.

REFERENCES

[1] W. Nie, H. Tsai, R. Asadpour, J.-C. Blancon, A.J. Neukirch, G. Gupta, et al. High-efficiency solution-processed perovskite solar cells with millimeter-scale grains. Science 2015; 347:522–525.

[2] O. Ergen, S.M. Gilbert, T. Pham, S.J. Turner, M.T.Z. Tan, M.A. Worsley, et al. Graded bandgap perovskite solar cells. Nat. Mater. 2016; 16:522–525.

[3] N.J. Jeon, J.H. Noh, Y.C. Kim, W.S. Yang, S. Ryu, S.I. Seok. Solvent engineering for high-performance inorganic–organic hybrid perovskite solar cells. Nat. Mater. 2014; 13:897–903.

[4] M. Xiao, F. Huang, W. Huang, Y. Dkhissi, Y. Zhu, J. Etheridge, et al. A Fast Deposition-Crystallization Procedure for Highly Efficient Lead Iodide Perovskite Thin-Film Solar Cells. Angew. Chem. Int. Ed. 2014; 53:9898–9903

[5] C. Zuo, L. Ding. An 80.11% FF record achieved for perovskite solar cells by using the NH_4Cl additive. Nanoscale 2014; 6:9935.

[6] P.-W. Liang, C.-Y. Liao, C.-C. Chueh, F. Zuo, S.T. Williams, X.-K. Xin, et al. Additive Enhanced Crystallization of Solution-Processed Perovskite for Highly Efficient Planar-Heterojunction Solar Cells. Adv. Mater. 2014; 26:3748–3754.

[7] J.-H. Im, I.-H. Jang, N. Pellet, M. Grätzel, N.-G. Park. Growth of $CH_3NH_3PbI_3$ cuboids with controlled size for high-efficiency perovskite solar cells. Nat. Nanotechnol. 2014; 9:927–932.

[8] W.S. Yang, J.H. Noh, N.J. Jeon, Y.C. Kim, S. Ryu, J. Seo, et al. High-performance photovoltaic perovskite layers fabricated through intramolecular exchange. Science. 2015; 348:1234–1237.

[9] X. Li, J. Yang, Q. Jiang, W. Chu, D. Zhang, Z. Zhou, et al. Enhanced photovoltaic performance and stability in mixed-cation perovskite solar cells via compositional modulation. Electrochim. Acta 2017; 247:460–467.

[10] W. Zhang, S. Pathak, N. Sakai, T. Stergiopoulos, P.K. Nayak, N.K. Noel, et al. Enhanced optoelectronic quality of perovskite thin films with hypophosphorous acid for planar heterojunction solar cells. Nat. Commun. 2015; 6:10030.

[11] Q. Hu, J. Wu, C. Jiang, T. Liu, X. Que, R. Zhu, et al. Engineering of Electron-Selective Contact for Perovskite Solar Cells with Efficiency Exceeding 15%. ACS Nano 2014; 8:10161–10167.

[12] B. Wang, Z.-G. Zhang, S. Ye, L. Gao, T. Yan, Z. Bian, et al. Solution-Processable Cathode Buffer Layer for High-Performance ITO/CuSCN-based Planar Heterojunction Perovskite Solar Cell. Electrochim. Acta 2016; 218:263–270.

[13] A.S. Subbiah, A. Halder, S. Ghosh, N. Mahuli, G. Hodes, S.K. Sarkar. Inorganic Hole Conducting Layers for Perovskite-Based Solar Cells. J. Phys. Chem. Lett. 2014; 5:1748–1753.

[14] J.H. Heo, S.H. Im, J.H. Noh, T.N. Mandal, C.-S. Lim, J.A. Chang, et al. Efficient inorganic–organic hybrid heterojunction solar cells containing perovskite compound and polymeric hole conductors. Nat. Photonics 2013; 7: 486–491.

[15] S. Liu, R. Liu, Y. Chen, S. Ho, J.H. Kim, F. So. Nickel Oxide Hole Injection/Transport Layers for Efficient Solution-Processed Organic Light-Emitting Diodes. Chem. Mater 2014; 26:4528–4534.

[16] M.S. Ryu, J. Jang. Enhanced efficiency of organic photovoltaic cells using solution-processed metal oxide as an anode buffer layer. Sol. Energy Mater. Sol. Cells 2011; 95:3015–3020.

[17] W. Chen et al. Efficient and stable large-area perovskite solar cells with inorganic charge extraction layers. Science 2015; 350:944–948.

[18] J. A. Christians, R. C. M. Fung, P. V. Kamat, J. Am. An Inorganic Hole Conductor for Organo-Lead Halide Perovskite Solar Cells. Improved Hole Conductivity with Copper Iodide. Chem. Soc. 2014; 136:758–764.

[19] I. Chung, B. Lee, J. He, R. P. H. Chang, M. G. Kanatzidis. All-solid-state dye-sensitized solar cells with high efficiency. Nature 2012; 485:486–489.

[20] P. Qin et al. Inorganic hole conductor-based lead halide perovskite solar cells with 12.4% conversion efficiency. Nat. Commun. 2014; 5:3834.

[21] J. E. Jaffe et al. Electronic and Defect Structures of CuSCN. J. Phys. Chem. C 2010; 114:9111–9117.

[22] J. W. Jung, C.-C. Chueh, A. K. Y. Jen. A Low-Temperature, Solution-Processable, Cu-Doped Nickel Oxide Hole-Transporting Layer via the Combustion Method for High-Performance Thin-Film Perovskite Solar Cells. Adv. Energy Mater. 2015; 5:7874–7880.

[23] S. Ye et al. CuSCN-Based Inverted Planar Perovskite Solar Cell with an Average PCE of 15.6%. Nano Lett. 2015; 15:3723–3728.

[24] N. Arora et al. Perovskite solar cells with CuSCN hole extraction layers yield stabilized efficiencies greater than 20%. Science 2017; 10.1126/ science.aam5655

[25] M. Jung et al. Thermal Stability of CuSCN Hole Conductor-Based Perovskite Solar Cells. ChemSusChem 2016; 9:2592–2596.

[26] J. Liu et al. Copper Thiocyanate: An Efficient and Affordable Hole Transporting Material, toward Thermally Stable Perovskite Solar Cells. Adv. Mater. Interfaces 2016; 3:1600571.

[27] S. Ye et al. A Strategy to Simplify the Preparation Process of Perovskite Solar Cells by Co-deposition of a Hole-Conductor and a Perovskite Layer. Adv. Mater. 2016; 28:9648–9654.

[28] V. E. Madhavan et al. Copper Thiocyanate Inorganic Hole-Transporting Material for High-Efficiency Perovskite Solar Cells. ACS Energy Lett. 2016; 1:1112 –1117.

[29] N. Yaacobi-Gross et al. High-Efficiency Organic Photovoltaic Cells Based on the Solution-Processable Hole Transporting Interlayer Copper Thiocyanate (CuSCN) as a Replacement for PEDOT:PSS. Adv. Energy Mater. 2015; 5:1401529.

[30] D. M. Chapin, C. S. Fuller, and G. L. Pearson. A new silicon p-n junction photocell for converting solar radiation into electrical power. J. Appl. Phys. 1954; 25(5):676–677.

[31] Fraunhofer Institute for Solar Energy Systems, "Photovoltaic report," 2015, https://www.ise.fraunhofer.de/de/downloads/pdffiles/aktuelles/photovoltaics -report-in-englischersprache.pdf (29 March 2018).

[32] M.A.Green et al. Solar cell efficiency tables (version47). Prog.Photovolt. 2016; 24(1):3–11.

[33] H. J. Snaith. Perovskites: the emergence of a new era for low-cost, high-efficiency solar cells. J. Phys. Chem. Lett. 2013; 4(21):3623–3630.

[34] N.-G. Park. Organometal perovskite light absorbers toward a 20% efficiency low-cost solid-state mesoscopic solar cell. J. Phys. Chem. Lett. 2013; 4(15):2423–2429.

[35] R. F. Service. Perovskite solar cells keep on surging. Science. 2014; 344(6183):458.

[36] M. A. Green, A. Ho-Baillie, and H. J. Snaith. The emergence of perovskite solar cells. Nat. Photon. 2014; 8(7):506–514.

[37] M. Gratzel. The light and shade of perovskite solar cells. Nat. Mater. 2014; 13(9):838–842.

[38] P. Gao, M. Gratzel, and M. K. Nazeeruddin. Organohalide lead perovskites for photovoltaic applications. Energy Environ. Sci. 2014; 7(8):2448–2463.

[39] S. D. Stranks and H. J. Snaith. Metal-halide perovskites for photovoltaic and light-emitting devices. Nat. Nanotechnol. 2015; 10(5):391–402.

[40] Q. Chen et al. Under the spotlight: the organic-inorganic hybrid halide perovskite for optoelectronic applications. Nano Today. 2015; 10(3):355–396.

[41] T. C. Sumand N. Mathews. Advancements inperovskite solar cells: photophysics behind the photovoltaics. Energy Environ. Sci. 2014; 7(8): 2518–2534.

[42] A. K. Chilvery et al. Perovskites: transforming photovoltaics, a mini-review. J. Photon. Energy. 2015; 5(1):057402.

[43] L. J. Schmidt. Tracking down the truth of perovski. in 38th Rochester Mineralogical Symp. Program Notes. 2011: 31–32.

[44] D. B. Mitzi. Synthesis, crystal structure, and optical and thermal properties of $(C_4H_9NH_3)_2MI_4$ (M=Ge, Sn, Pb). Chem. Mater. 1996; 8(3): 791–800.

[45] D. B. Mitzi, M. T. Prikas, and K. Chondroudis. Thin filmdeposition of organic-inorganic hybrid materials using a single source thermal ablation technique. Chem. Mater. 1999; 11(3):542–544.

[46] D. B. Mitzi, C. D. Dimitrakopoulos, and L. L. Kosbar. Structurally tailored organic-inorganic perovskites: optical properties and solution processed channel materials for thin-film transistors. Chem. Mater. 2001; 13(10):3728–3740.

[47] J. Calabrese et al. Preparation and characterization of layered lead halide compounds. J. Am. Chem. Soc. 1991; 113(6):2328–2330.

[48] K. Chondroudis and D. B. Mitzi. Electroluminescence from an organic-inorganic perovskite incorporating a quaterthiophene dye within lead halide perovskite layers. Chem. Mater. 1999; 11(11):3028–3030.

[49] D. B. Mitzi, K. Chondroudis, and C. R. Kagan. Organic-inorganic electronics. IBM J. Res. Dev. 2001; 45(1): 29–45.

[50] Henry J. Snaith. Perovskites: The Emergence of a New Era for Low-Cost, High Efficiency Solar Cells. J. Phys. Chem. Lett. 2013; 4:3623−3630.

[51] A. Kojima et al. Organometal halide perovskites as visible-light sensitizers for photovoltaic cells. J. Am. Chem. Soc. 2009; 131(17):6050–6051.

[52] Editorial. Perovskite fever. Nat. Mater. 2014; 13(9):837.

[53] H.-S. Kim et al. Lead iodide perovskite sensitized all-solid-state submicron thin film mesoscopic solar cell with efficiency exceeding 9%. Sci. Rep. 2012; 2:591.

[54] M. M. Lee et al. Efficient hybrid solar cells based on meso-superstructured organometal halide perovskites. Science. 2012; 338(6107):643–647.

[55] NREL. "Solar cell efficiency chart," http://www.nrel.gov/ncpv/images/efficiency_chart. jpg (09 March 2016).

[56] J. Burschka et al. Sequential deposition as a route to high-performance perovskite-sensitized solar cells. Nature. 2013; 499(7458):316–319.

[57] M. Liu, M. B. Johnston, and H. J. Snaith. Efficient planar heterojunction perovskite solar cells by vapour deposition. Nature. 2013; 501(7467): 395–398.

[58] Q. Chen et al. Planar heterojunction perovskite solar cells via vapor-assisted solution process. J. Am. Chem. Soc. 2014; 136(2):622–625.

[59] C.-W. Chen et al. Efficient and uniform planar-type perovskite solar cells by simple sequential vacuum deposition. Adv. Mater. 2014; 26(38):6647–6652.

[60] J. H. Noh et al. Chemical management for colorful, efficient, and stable inorganicorganic hybrid nanostructured solar cells. Nano Lett. 2013; 13(4):1764–1769.

[61] G. E. Eperon et al. Formamidinium lead trihalide: a broadly tunable perovskite for efficient planar heterojunction solar cells. Energy Environ. Sci. 2014; 7(3): 982–988.

[62] W. J. Yin, T. T. Shi, and Y. F. Yan. Unique properties of halide perovskites as possible origins of the superior solar cell performance. Adv. Mater. 2014; 26(27):4653–4658.

[63] S.DeWolfetal. Organo metallic halide perovskites: sharp optical absorption edge and its relation to photovoltaic performance. J. Phys. Chem. Lett. 204; 5(6):1035–1039.

[64] C. S. Ponseca, Jr. et al. Organometal halide perovskite solar cell materials rationalized: ultrafast charge generation, high and microsecond-long balanced mobilities, and slow recombination. J. Am. Chem. Soc. 2014; 136(14): 5189–5192.

[65] V. D'Innocenzo et al. Excitons versus free charges in organo-lead tri-halide perovskites. Nat. Commun. 2014; 5: 3586.

[66] S. D. Stranks et al. Recombination kinetics in organic-inorganic perovskites: excitons, free charge, and subgap states. Phys. Rev. Appl. 2014; 2(3):034007.

[67] S.D.Stranksetal. Electron hole diffusion lengths exceeding 1 micro meter in an organo metal tri halide perovskite absorber. Science. 2013; 342(6156): 341–344.

[68] G. Xing et al. Long-range balanced electron- and hole-transport lengths in organic-inorganic $CH_3NH_3PbI_3$. Science. 2013; 342(6156):344–347.

[69] C. Wehrenfennig et al. High charge carrier mobilities and lifetimes in organolead trihalide perovskites. Adv. Mater. 2014; 26(10):1584–1589.

[70] T. Leijtens et al. Electronic properties of meso-superstructured and planar organometal halide perovskite films: charge trapping, photodoping, and carrier mobility. ACS Nano. 2014; 8(7):7147–7155.

[71] W.J. Yin, T. Shi, and Y. Yan. Unusual defect physics in $CH_3NH_3PbI_3$ perovskite solar cell absorber. Appl. Phys. Lett. 2014; 104(6): 063903.

[72] W. Tress et al. Predicting the open-circuit voltage of $CH_3NH_3PbI_3$ perovskite solar cells using electroluminescence and photovoltaic quantum efficiency spectra: the role of radiative and non-radiative recombination. Adv. Energy Mater. 2015; 5(3): 1400812.

[73] J. H. Im et al. 6.5% efficient perovskite quantum-dot-sensitized solar cell. Nanoscale. 2011; 3(10):4088–4093.

[74] B.O'Regan and M.Gratzel. Alow-cost, high-efficiency solar cell based on dye-sensitized colloidal TiO_2 films. Nature. 1991; 353(6346):737–740.

[75] W. Chen et al. Hybrid interfacial layer leads to solid performance improvement of inverted perovskite solar cells. Energy Environ. Sci. 2015; 8(2): 629–640.

[76] K. C. Wang et al. P-type mesoscopic nickel oxide/organometallic perovskite heterojunction solar cells. Sci. Rep. 2014; 4: 4756.

[77] M. Lee et al. Efficient, durable and flexible perovskite photovoltaic devices with Ag embedded ITO as the top electrode on a metal substrate. J. Mater. Chem. A. 2015; 3(28):14592–14597.

[78] J. Troughton et al. Highly efficient, flexible, indium-free perovskite solar cells employing metallic substrates. J. Mater. Chem. A. 2015; 3(17):9141–9145.

[79] J. H. Heo et al. Efficient inorganic-organic hybrid heterojunction solar cells containing perovskite compound and polymeric hole conductors. Nat.Photon. 2013; 7(6):486–491.

[80] J. J. Choi et al. Structure of methyl ammonium lead iodide within mesoporous titanium dioxide: active material in high-performance perovskite solar cells. Nano Lett. 2014; 14(1):127–133.

[81] T. Leijtens et al. Overcoming ultraviolet light instability of sensitized TiO_2 with mesosuperstructured organometal tri-halide perovskite solar cells. Nat. Commun. 2013; 4: 2885.

[82] T. Leijtens et al. The importance of perovskite pore filling in organometal mixed halide sensitized TiO_2-based solar cells. J. Phys. Chem. Lett. 2014; 5(7): 1096–1102.

[83] G. E. Eperon et al. Morphological control for high performance, solution-processed planar heterojunction perovskite solar cells Adv. Funct. Mater. 2014; 24(1):151–157.

[84] W. S. Yang et al. High-performance photovoltaic perovskite layers fabricated through intramolecular exchange. Science. 2015; 348(6240):1234–1237.

[85] E.Edrietal. Why lead methyl ammonium tri-iodide perovskite-based solar cells require a mesoporous electron transporting scaffold (but not necessarily a hole conductor). Nano Lett. 2014; 14(2):1000–1004.

[86] H. Zhou et al. Interface engineering of highly efficient perovskite solar cells. Science. 2014; 345(6196):542–546.

[87] J.Y. Jeng et al. $CH_3NH_3PbI_3$ perovskite / fullerene planar-heterojunction hybrid solar cells. Adv. Mater. 2013; 25(27): 3727–3732.

[88] O. Malinkiewicz et al. Perovskite solar cells employing organic charge-transport layers. Nat. Photon. 2014; 8(2):128–132.

[89] Q. Dong et al. Abnormal crystal growth in $CH_3NH_3PbI_{3-x}Cl_x$ using a multi-cycle solution coating process. Energy Environ. Sci. 2015; 8(8):2464–2470.

[90] W. Chen et al. Efficient and stable large-area perovskite solar cells with inorganic charge extraction layers. Science. 2015; 350(6263): 944–948.

[91] J. You et al. Improved air stability of perovskite solar cells via solution-processed metal oxide transport layers. Nat. Nanotechnol. 2016; 11(1): 75–81.

[92] J. H. Park et al. Efficient $CH_3NH_3PbI_3$ perovskite solar cells employing nanostructured p-type nio electrode formed by a pulsed laser deposition. Adv. Mater. 2015; 27(27):4013–4019.

[93] Z. Song et al. Impact of processing temperature and composition on the formation of methylammonium lead iodide perovskites. Chem. Mater. 2015; 27(13): 4612–4619.

[94] C. Roldan-Carmona et al. High efficiency methyl ammonium lead tri iodide perovskite solar cells: the relevance of non-stoichiometric precursors. Energy Environ. Sci. 2015; 8(12): 3550–3556.

[95] Q. Wang et al. Large fill-factor bilayer iodine perovskite solar cells fabricated by a lowtemperature solution-process. Energy Environ. Sci. 2014; 7(7):2359–2365.

[96] J.-H. Im et al. Growth of $CH_3NH_3PbI_3$ cuboids with controlled size for high-efficiency perovskite solar cells. Nat. Nanotechnol. 2014; 9(11):927–932.

[97] N.Ahn et al. Highly reproducible perovskite solar cells with average efficiency of 18.3% and best efficiency of 19.7% fabricated via Lewis base adduct of lead(II) iodide. J. Am. Chem. Soc. 2015; 137(27): 8696–8699.

[98] A. T. Barrows et al. Efficient planar heterojunction mixed-halide perovskite solar cells deposited via spray-deposition. Energy Environ. Sci. 2014; 7(9):2944–2950.

[99] Y. H. Deng et al. Scalable fabrication of efficient organolead trihalide perovskite solar cells with doctor-bladed active layers. Energy Environ. Sci. 2015; 8(5):1544–1550.

[100] S.-G. Li et al. Inkjet printing of $CH_3NH_3PbI_3$ on a mesoscopic TiO_2 film for highly efficient perovskite solar cells. J. Mater. Chem. A. 2015; 3(17):9092–9097.

[101] K. Hwang et al. Toward large scale roll-to-roll production of fully printed perovskite solar cells. Adv. Mater. 2015; 27(7): 1241–1247.

[102] K. N. Liang, D. B. Mitzi, and M. T. Prikas. Synthesis and characterization of organicinorganic perovskite thin films prepared using a versatile two-step dipping technique. Chem. Mater. 1998; 10(1): 403–411.

[103] Z.Song et al. Spatially resolved characterization of solution processed perovskite solar cells using the lbic technique. in IEEE 42nd Photovoltaic Specialist Conf. 2015: 1 –5.

[104] T. Zhang et al. Controllable sequential deposition of planar $CH_3NH_3PbI_3$ perovskite films via adjustable volume expansion. Nano Lett. 2015; 15(6): 3959–3963.

[105] N. J. Jeon et al. Solvent engineering for high-performance inorganic-organic hybrid perovskite solar cells. Nat. Mater. 2014; 13(9): 897–903.

[106] V. Nicolosi et al. Liquid exfoliation of layered materials. Science. 2013; 340(6139): 1226419.

[107] F. Hao et al. Controllable perovskite crystallization at a gas-solid interface for hole conductor-free solar cells with steady power conversion efficiency over 10%. J. Am. Chem. Soc. 2014; 136(46): 16411–16419.

[108] M. M. Tavakoli et al. Fabrication of efficient planar perovskite solar cells using a one step chemical vapor deposition method. Sci. Rep. 2015; 5: 14083.

[109] Q. Lin etal. Electro-optics of perovskite solar cells. Nat. Photon. 2015; 9(2): 106–112.

[110] D. Zhao et al. Annealing-free efficient vacuum-deposited planar perovskite solar cells with evaporated fullerenes as electron-selective layers. Nano Energy. 2016; 19: 88 –97.

[111] G. C. Papavassiliou. Three- and low-dimensional inorganic semiconductors. Prog. Solid State Chem. 1997; 25:125–270.

[112] T. Ishihara. Optical properties of PbI-based perovskite structures. J. Lumin. 1994; 60: 269–274.

[113] D. B. Mitzi. Templating and structural engineering in organic–inorganic perovskites. J. Chem. Soc. 2001; 1: 1–12.

[114] C. C. Stoumpos, C. D. Malliakas, and M. G. Kanatzidis. Semiconducting tin and lead iodide perovskites with organic cations: phase transitions, high mobilities, and near-infrared photoluminescent properties. Inorg.Chem. 2013; 52:9019–9038.

[115] J. H Heo et al. Efficient inorganic–organic hybrid heterojunction solar cells containing perovskite compound and polymeric hole conductors. Nature Photon. 2013; 7: 486–491.

[116] D. Bi, L.Yang, G.Boschloo, A. Hagfeldt, and E.M.J. Johansson. Effect of different hole transport materials on recombination in $CH_3NH_3PbI_3$ perovskite sensitized mesoscopic solar cells. J. Phys. Chem. Lett. 2013; 4: 1532–1536.

[117] M. M. Lee, J. Teuscher, T. Miyasaka, T. N. Murakami, and H. J. Snaith. Efficient hybrid solar cells based on meso-superstructured organometal halide perovskites. Science. 2012; 338: 643–647.

[118] M. Liu, M. B. Johnston, and H. J. Snaith. Efficient planar heterojunction perovskite solar cells by vapour deposition. Nature. 2013; 501: 395–398.

[119] W. Tress, N. Marinova, O. Inganäs, M.K. Nazeeruddin, S.M. Zakeeruddin, M. Graetzel. The role of the hole-transport layer in perovskite solar cells-reducing recombination and increasing absorption. in: IEEE Proceedings of the 40th Photovoltaic Specialist Conference (PVSC). 2014: 1563–1566.

[120] L. Zhu, J. Xiao, J. Shi, J. Wang, S. Lv, Y. Xu, Y. Luo, Y. Xiao, S. Wang, Q. Meng, X. Li, D. Li. Efficient $CH_3NH_3PbI_3$ perovskite solar cells with 2TPA-n-DP hole transporting layers. Nano Res. 2015; 8:1116–1127.

[121] S. Chen, Y. Hou, H. Chen, M. Richter, F. Guo, S. Kahmann, X. Tang, T. Stubhan, H. Zhang, N. Li, N. Gasparini, C.O.R. Quiroz, L.S. Khanzada, G.J. Matt, A. Osvet, C.J. Brabec. Exploring the limiting open-circuit voltage and the voltage loss mechanism in planar $CH_3NH_3PbBr_3$ perovskite solar cells. Adv. Energy Mater. 2016; 6:1600132.

[122] N.K. Elumalai, A. Uddin. Open circuit voltage of organic solar cells: an in-depth review. Energy Environ. Sci. 2016; 9: 391–410.

[123] Y. Shao, Y. Yuan, J. Huang. Correlation of energy disorder and open-circuit voltage in hybrid perovskite solar cells. Nat. Energy. 2016; 1: 15001.

[124] W. Tress. Maximum efficiency and open-circuit voltage of perovskite solar cells, in: N.-G. Park, M. Grätzel, T. Miyasaka (Eds.). Organic-Inorganic Halide Perovskite Photovoltaics: From Fundamentals to Device Architectures, Springer International Publishing, Switzerland, 2016: 53–77.

[125] H. Back, G. Kim, J. Kim, J. Kong, T.K. Kim, H. Kang, H. Kim, J. Lee, S. Lee, K. Lee. Achieving long-term stable perovskite solar cells via ion neutralization. Energy Environ. Sci. 2016; 9:1258–1263.

[126] Y. Kato, L.K. Ono, M.V. Lee, S. Wang, S.R. Raga, Y. Qi. Silver iodide formation in methyl ammonium lead iodide perovskite solar cells with silver top electrodes. Adv. Mater. Interfaces. 2015; 2: 1500195.

[127] E. Edri, S. Kirmayer, M. Kulbak, G. Hodes, D. Cahen. Chloride inclusion and hole transport material doping to improve methyl ammonium lead bromide perovskite-based high open-circuit voltage solar cells. J. Phys. Chem. Lett. 2014; 5: 429–433.

[128] C.G. Wu, C.H. Chiang, S.H. Chang. A perovskite cell with a record-high-Voc of 1.61 V based on solvent annealed $CH_3NH_3PbBr_3$/ICBA active layer. Nanoscale.2016; 8:4077–4085.

[129] J. You, L. Meng, T.-B. Song, T.-F. Guo, Y.M. Yang, W.-H. Chang, Z. Hong, H. Chen, H. Zhou, Q. Chen, Y. Liu, N.D. Marco, Y. Yang. Improved air stability of perovskite solar cells via solution-processed metal oxide transport layers. Nat. Nanotechnol. 2016; 11:75–81.

[130] F. Di Giacomo, A. Fakharuddin, R. Jose, T.M. Brown. Progress, challenges and perspectives in flexible perovskite solar cells. Energy Environ. Sci. 2016; 9: 3007–3035.

[131] J.A. Christians, P.V. Kamat. Trap and transfer. Two-step hole injection across the Sb_2S_3/CuSCN interface in solid-state solar cells. ACS Nano. 2013; 7: 7967–7974.

[132] B. Li, L. Wang, B. Kang, P. Wang, Y. Qiu. Review of recent progress in solid-state dye-sensitized solar cells. Sol. Energy Mater. Sol. Cells 2006; 90: 549–573.

[133] M. Rusop, T. Soga, T. Jimbo, M. Umeno. Copper Iodide thin films as a p-TYPE electrical conductivity in dye-sensitized p-CuI/Dye/n-TiO_2 heterojunction solid state solar cells. Surf. Rev. Lett. 2004; 11:577.

[134] J.A. Chang, S.H. Im, Y.H. Lee, H.J. Kim, C.S. Lim, J.H. Heo, S.I. Seok. Panchromatic photon-harvesting by hole-conducting materials in inorganic-organic heterojunction sensitized-solar cell through the formation of nanostructured electron channels. Nano Lett. 2012; 12: 1863–1867.

[135] S. Nezu, G. Larramona, C. Choné, A. Jacob, B. Delatouche, D. Péré, C. Moisan. Light soaking and gas effect on nanocrystalline TiO_2/Sb_2S_3/CuSCN photovoltaic cells following extremely thin absorber concept. J. Phys. Chem. C. 2010; 114:6854–6859.

[136] Z. H. Bakra, Q. Walia, A. Fakharuddinc, L. Schmidt-Mendec, T. M. Browne, and R. Josea. Advances in hole transport materials engineering for stable and efficient perovskite solar cells. Nano Energy. 2017; 34: 271–305.

[137] N. Ahn, D.-Y. Son, I.-H. Jang, S.M. Kang, M. Choi, N.-G. Park. Highly reproducible perovskite solar cells with average efficiency of 18.3% and best

efficiency of 19.7% fabricated via Lewis base adduct of lead (II) iodide. J. Am. Chem. Soc. 2015; 137:8696–8699.

[138] I. Mcculloch, M. Heeney, C. Bailey, K. Genevicius, I. Macdonald, M. Shkunov, D. Sparrowe, S. Tierney, R. Wagner, W. Zhang, M.L. Chabinyc, R.J. Kline, M.D. Mcgehee, M.F. Toney. Liquid-crystalline semiconducting polymers with high charge-carrier mobility. Nat. Mater. 2006; 5:328–333.

[139] S.N. Habisreutinger, T. Leijtens, G.E. Eperon, S.D. Stranks, R.J. Nicholas, H.J. Snaith. Carbon nanotube/polymer composites as a highly stable hole collection layer in perovskite solar cells. Nano Lett. 2014; 14: 5561–5568.

[140] W.S. Yang, J.H. Noh, N.J. Jeon, Y.C. Kim, S. Ryu, J. Seo, S.I. Seok. High performance photovoltaic perovskite layers fabricated through intramolecular exchange. Science. 2015; 348: 1234–1237.

[141] J.H. Heo, H.J. Han, D. Kim, T.K. Ahn, S.H. Im, Hysteresis-less inverted $CH_3NH_3PbI_3$ planar perovskite hybrid solar cells with 18.1% power conversion efficiency, Energy Environ. Sci. 2015; 8: 1602–1608.

[142] W.-Y. Chen, L.-L. Deng, S.-M. Dai, X. Wang, C.-B. Tian, X.-X. Zhan, S.-Y. Xie, R.B. Huang, L.-S. Zheng. Low-cost solution-processed copper iodide as an alternative to PEDOT: pss hole transport layer for efficient and stable inverted planar heterojunction perovskite solar cells. J. Mater. Chem. A. 2015; 3:19353–19359.

[143] S. Ye, W. Sun, Y. Li, W. Yan, H. Peng, Z. Bian, Z. Liu, C. Huang. CuSCN-based inverted planar perovskite solar cell with an average PCE of 15.6%. Nano Lett. 2015; 15: 3723–3728.

[144] J.H. Park, J. Seo, S. Park, S.S. Shin, Y.C. Kim, N.J. Jeon, H.-W. Shin, T.K. Ahn, J.H. Noh, S.C. Yoon, C.S. Hwang, S.I. Seok. Efficient $CH_3NH_3PbI_3$ perovskite solar cells employing nanostructured p-Type NiO electrode formed by a pulsed laser deposition. Adv. Mater. 2015; 27: 4013–4019.

[145] C. Zuo, L. Ding. Solution-processed Cu_2O and CuO as hole transport materials for efficient perovskite solar cells. Small. 2015; 11: 5528–5532.

[146] W. Li, H. Dong, X. Guo, N. Li, J. Li, G. Niu, L. Wang. Graphene oxide as dual functional interface modifier for improving wettability and retarding

recombination in hybrid perovskite solar cells. J. Mater. Chem. A. 2014; 2: 20105–20111.

[147] J. E. Jaffe, T. C. Kaspar, T. C. Droubay, T. Varga, M. E. Bowden, G. J. Exarhos. Electronic and Defect Structures of CuSCN. J. Phys. Chem. C. 2010; 114: 9111.

[148] P. Pattanasattayavong, N. Yaacobi-Gross, K. Zhao, G. O. N. Ndjawa, J. Li, F. Yan, B. C. O'Regan, A. Amassian, T. D. Anthopoulos. Hole-Transporting Transistors and Circuits Based on the Transparent Inorganic Semiconductor Copper(I) Thiocyanate (CuSCN) Processed from Solution at Room Temperature. Adv. Mater. 2013; 25: 1504.

[149] P. Pattanasattayavong, A. D. Mottram, F. Yan, T. D. Anthopoulos. Study of the Hole Transport Processes in Solution-Processed Layers of the Wide Bandgap Semiconductor Copper(I) Thiocyanate (CuSCN). Adv. Funct. Mater. 2015; 25: 6802.

[150] L. Petti, P. Pattanasattayavong, Y. Lin, N. Münzenrieder, G. Cantarella, N. Yaacobi-Gross, F. Yan, G. Tröster, T. D. Anthopoulos. Solution-processed p-type copper(I) thiocyanate (CuSCN) for low-voltage flexible thin-film transistors and integrated inverter circuits. Appl. Phys. Lett. 2017; 110: 113504.

[151] N. Wijeyasinghe, T. D. Anthopoulos. Copper(I) thiocyanate (CuSCN) as a holetransport material for large-area optoelectronics. Semicond. Sci. Technol. 2015; 30: 104002.

[152] P. Pattanasattayavong, G. O. N. Ndjawa, K. Zhao, K. W. Chou, N. Yaacobi-Gross, B. C. O'Regan, A. Amassian, T. D. Anthopoulos. Electric field-induced hole transport in copper(I) thiocyanate (CuSCN) thin-films processed from solution at room temperature. Chem. Commun. 2013; 49: 4154.

[153] N. Yaacobi-Gross, N. D. Treat, P. Pattanasattayavong, H. Faber, A. K. Perumal, N. Stingelin, D. D. C. Bradley, P. N. Stavrinou, M. Heeney, T. D. Anthopoulos. High-Efficiency Organic Photovoltaic Cells Based on the Solution-Processable Hole Transporting Interlayer Copper Thiocyanate (CuSCN) as a Replacement for PEDOT:PSS. Adv. Energy Mater. 2015; 5: 1401529.

[154] N. D. Treat, N. Yaacobi-Gross, H. Faber, A. K. Perumal, D. D. C. Bradley, N. Stingelin, T. D. Anthopoulos. Copper thiocyanate: An attractive hole transport/extraction layer for use in organic photovoltaic cells. Appl. Phys. Lett. 2015; 107: 013301.

[155] P. Qin, S. Tanaka, S. Ito, N. Tetreault, K. Manabe, H. Nishino, M. K. Nazeeruddin, M. Gratzel. Inorganic hole conductor-based lead halide perovskite solar cells with 12.4% conversion efficiency. Nat. Commun. 2014; 5: 3834.

[156] K. Zhao, R. Munir, B. Yan, Y. Yang, T. Kim, A. Amassian. Solution-processed inorganic copper(I) thiocyanate (CuSCN) hole transporting layers for efficient p–i–n perovskite solar cells. J. Mater. Chem. A. 2015; 3: 20554.

[157] S. Ye, W. Sun, Y. Li, W. Yan, H. Peng, Z. Bian, Z. Liu, C. Huang. CuSCN-Based Inverted Planar Perovskite Solar Cell with an Average PCE of 15.6%. Nano Lett. 2015; 15: 3723.

[158] A. Perumal, H. Faber, N. Yaacobi-Gross, P. Pattanasattayavong, C. Burgess, S. Jha, M. A. McLachlan, P. N. Stavrinou, T. D. Anthopoulos, D. D. C. Bradley. High-Efficiency, Solution-Processed, Multilayer Phosphorescent Organic Light-Emitting Diodes with a Copper Thiocyanate Hole-Injection / Hole-Transport Layer. Adv. Mater. 2015; 27: 93.

[159] L.J. Xu, J.Y. Wang, X.F. Zhu, X.C. Zeng, Z.N. Chen. Phosphorescent Cationic Au_4Ag_2 Alkynyl Cluster Complexes for Efficient Solution-Processed Organic Light-Emitting Diodes. Adv. Funct. Mater. 2015; 25: 3033.

[160] X. Zhang, S. Yoshioka, N. Loew, M. Ihara. Microstructure control of absorber Sb2S3 and p-type semiconductor CuSCN for semiconductor-sensitized solar cells ($TiO_2/Sb_2S_3/CuSCN$). ECS Trans. 2014; 64 (15): 1.

[161] S. Yoshioka, T. Mishima, M. Ihara. The Effect of TiO_2 Microstructure and Introduction of Silver Nanoparticles on Conversion Efficiency of Sb_2S_3 Sensitized Semiconductor Solar Cells. ECS Trans. 2013; 50: 33.

[162] S. Ito, S. Tanaka, H. Vahlman, H. Nishino, K. Manabe, P. Lund. Carbon-Double-Bond-Free Printed Solar Cells from $TiO_2/CH_3NH_3PbI_3/CuSCN/Au$: Structural Control and Photoaging Effects. ChemPhysChem 2014; 15: 1194.

[163] E. Bacaksiz, S. Aksu, G. Çankaya, S. Yılmaz, I . Polat, T. Kücükömeroglu, A. Varilci. Fabrication of p-type CuSCN/n-type micro-structured ZnO heterojunction structures. Thin Solid Films. 2011; 519: 3679.

[164] S. M. Hatch, J. Briscoe, S. Dunn. Improved CuSCN-ZnO diode performance with spray deposited CuSCN. Thin Solid Films. 2013; 531: 404.

[165] Y. Selk, T. Yoshida, T. Oekermann. Variation of the morphology of electrodeposited copper thiocyanate films. Thin Solid Films. 2008; 516: 7120.

[166] W. Wu, Z. Jin, Z. Hua, Y. Fu, J. Qiu. Growth mechanisms of CuSCN films electrodeposited on ITO in EDTA-chelated copper(II) and KSCN aqueous solution. Electrochim. Acta. 2005; 50: 2343.

[167] B. O'Regan, D. T. Schwartz, S. M. Zakeeruddin, M. Grätzel. Electrodeposited Nanocomposite n–p Heterojunctions for Solid-State Dye-Sensitized Photovoltaics. Adv. Mater. 2000; 12: 1263.

[168] S.-Y. Sung, S.-Y. Kim, K.-M. Jo, J.-H. Lee, J.-J. Kim, S.-G. Kim, K.-H. Chai, S. J. Pearton, D. P. Norton, Y.-W. Heo. Fabrication of p-channel thin-film transistors using CuO active layers deposited at low temperature. Appl. Phys. Lett. 2010; 97: 222109.

[169] Zhaoning Song Suneth C. Watthage Adam B. Phillips Michael J. Hebe. Pathways toward high-performance perovskite solar cells: review of recent advances in organo-metal halide perovskites for photovoltaic applications. Journal of Photonics for Energy. 2016; 6(2).

[170] P. Pattanasattayavong, G.O.N. Ndjawa, K. Zhao, K.W. Chou, N. Yaacobi-Gross, B.C. O'regan, A. Amassian, T.D. Anthopoulos. Electric field-induced hole transport in copper (I) thiocyanate (CuSCN) thin-films processed from solution at room temperature. Chem. Commun. 2013; 49: 4154.

[171] P. Pattanasattayavong, N. Yaacobi-Gross, K. Zhao, G.O.N. Ndjawa, J. Li, F. Yan, B.C. O'regan, A. Amassian, T.D. Anthopoulos. Hole-transporting transistors and circuits based on the transparent inorganic semiconductor Copper (I) Thiocyanate (CuSCN) processed from solution at room temperature. Adv. Mater. 2013; 25: 1504.

[172] S. Chavhan, O. Miguel, H.-J. Grande, V. Gonzalez-Pedro, R.S. Sánchez, E.M. Barea, I. Mora-Seró, R. Tena-Zaera. Organo-metal halide perovskite-based

solar cells with CuSCN as the inorganic hole selective contact. J. Mater. Chem. A. 2014; 2: 12754.

[173] S. Ito, S. Tanaka, H. Vahlman, H. Nishino, K. Manabe, P. Lund. Carbon-doublebond-free printed solar cells from $TiO_2/CH_3NH_3PbI_3/CuSCN/Au$: structural control and photoaging effects. ChemPhysChem. 2014; 15: 1194–1200.

[174] S. Ito, S. Tanaka, K. Manabe, H. Nishino, Effects of surface blocking layer of Sb_2S_3 on nanocrystalline TiO_2 for $CH_3NH_3PbI_3$ perovskite solar cells, J. Phys. Chem. C. 2014; 118: 16995.

[175] A. Fakharuddin, F. Di Giacomo, I. Ahmed, Q. Wali, T.M. Brown, R. Jose. Role of morphology and crystallinity of nanorod and planar electron transport layers on the performance and long term durability of perovskite solar cells, J. Power Sources. 2015; 283: 61.

[176] A. Fakharuddin, F. Di Giacomo, A.L. Palma, F. Matteocci, I. Ahmed, S. Razza, A. D'epifanio, S. Licoccia, J. Ismail, A. Di Carlo, T.M. Brown, R. Jose. Vertical TiO_2 nanorods as a medium for stable and high-efficiency perovskite solar modules. ACS nano. 2015; 9: 8420.

[177] P. Qin, S. Tanaka, S. Ito, N. Tetreault, K. Manabe, H. Nishino, M.K. Nazeeruddin M. Grätzel. Inorganic hole conductor-based lead halide perovskite solar cells with 12.4% conversion efficiency. Nat. Commun. 2014; 5: 3834.

[178] A.S. Subbiah, A. Halder, S. Ghosh, N. Mahuli, G. Hodes, S.K. Sarkar. Inorganic hole conducting layers for perovskite-based solar cells. J. Phys. Chem. Lett. 2014; 5: 1748.

[179] J.W.Lee, H.S. Kim, Nam-Gyu Park. Lewis Acid−Base Adduct Approach for High Efficiency Perovskite Solar Cells, Acc. Chem. Res. 2016; 49: 311.

[180] Nam-Gyu Park. Methodologies for high efficiency perovskite solar cells. Park Nano Convergence. 2016; 3: 15.

[181] J. E. Jaffe et al., Electronic and Defect Structures of CuSCN. J. Phys. Chem. C. 2010;114: 9111.

[182] D. Cahen, A. Kahn. Electron Energetics at Surfaces and Interfaces: Concepts and Experiments. Advanced Materials 2003; 15:271–277.

[183] R. C. Neville, Solar Energy Conversion The Solar Cell 2nd Edition, Elsevier Science B.VA., Amsterdam, 1995.

[184] W.A. Laban, L. Etgar. Depleted hole conductor-free lead halide iodide heterojunction solar cells. Energy Environ. Sci. 2013; 6:3249.

[185] J. Shi, J. Dong, S. Lv, Y. Xu, L. Zhu, J. Xiao, et al. Hole-conductor-free perovskite organic lead iodide heterojunction thin-film solar cells: High efficiency and junction property. Appl. Phys. Lett. 2014; 104:063901.

[186] W. Tress, A. Petrich, M. Hummert, M. Hein, K. Leo, M. Riede. Imbalanced mobilities causing S-shaped IV curves in planar heterojunction organic solar cells. Appl. Phys. Lett. 2011; 98:063301.

[187] H.-S. Kim, I. Mora-Sero, V. Gonzalez-Pedro, F. Fabregat-Santiago, E.J. Juarez-Perez, N.-G. Park, et al. Mechanism of carrier accumulation in perovskite thin-absorber solar cells. Nat. Commun. 2013; 4.

[188] J.A. Christians, R.C.M. Fung, P.V. Kamat. An Inorganic Hole Conductor for Organo-Lead Halide Perovskite Solar Cells. Improved Hole Conductivity with Copper Iodide. J. Am. Chem. Soc. 2014; 136:758–764.

[189] D. Liu, J. Yang, T.L. Kelly. Compact Layer Free Perovskite Solar Cells with 13.5% Efficiency. J. Am. Chem. Soc. 2014; 136:17116–17122.